METEOR-Berichte

Structural evolution and disintegration of oceanic intraplate volcanoes: The Bathymetrists Seamounts and its relation to Sierra Leona Rise (eastern equatorial Atlantic)

Cruise No. M152/2

03.01. – 12.02.2019

Las Palmas (Spain) – Walvis Bay (Namibia)

SEDIS

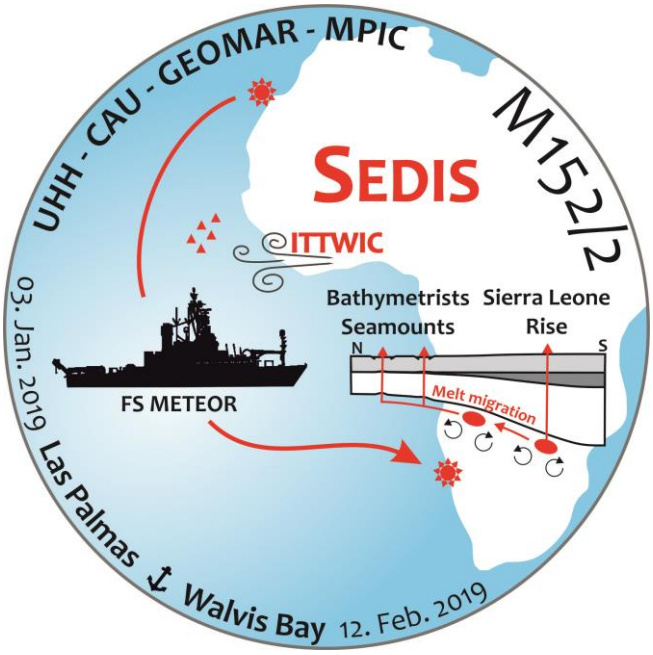

Christian Hübscher, Froukje van der Zwan, Henrik Grob, Tobias Häcker, Matthias Hartge, Hendrik Huster, Lisett Kretzschmann, Danai Lampridou, Frank Otte, Jonas Preine, Andreas Raeke, Wiebke Schäfer, Martin Schade, Elisabeth Seidel, Arne Warwel, Lena Wehmeier, Sven Winter

Chief Scientist: Christian Hübscher

University of Hamburg

2019

Table of Contents

1 Cruise Summary

(C. Hübscher, F. van der Zwan)

Summary

The Bathymetrists Seamounts (BSM) are located north of the volcanic Sierra Leone Rise in the eastern Atlantic between 6° and 9°N. The three W-E, N-S and NE-SW striking directions of the seamounts indicate a clear structural control for the emplacement of these volcanoes. The origin of the melts, their relationship to the Sierra Leone Rise and the role of the faults in the formation of the melts are unknown as the BSM could be explained by plume related volcanism or decompression melting beneath deep (transform) faults. The SEDIS-cruise M152/2 of RV METEOR strove for a better understanding of the life cycle of submarine volcanoes and their effect on the oceanic lithosphere in the oceanic intraplate setting of the BSM and the relationship to the Sierra Leone Rise. The aims were: 1) to understand the interaction between crustal thickness, tectonics and volcanic phases, 2) to investigate the structural, chronological and petrological evolution of individual seamounts and seamount chains, 3) to review slope failures and resulting mass flow processes. We addressed these objectives by more than 4000 km high-resolution reflection seismic and more than 5000 km of parametric echosounder, multi-beam, and gravity and magnetic profiles. Rock samples for ground truthing and geochemical research have been collected during 14 dredge stations. We further determined the concentrations in surface seawater and air and the state of air-sea exchange of a number of nowadays globally banned pesticides, polychlorinated biphenyls, brominated flame retardants, polycyclic aromatic hydrocarbons and their derivatives.

Zusammenfassung

Die Bathymetrists Seeberge liegen nördlich der Sierra Leone Schwelle, einer vulkanischen Plattform im östlichen Atlantik zwischen 6° und 9° N. Diese submarinen Vulkane gruppieren sich entlang W-E, N-S und NE-SW Trends, was eine strukturelle Kontrolle der Vulkanentstehung indiziert. Die Schmelzentstehung sind unbekannt und können mit Plume-Vulkanismus oder Dekompressionsschmelzen unter bisher nicht untersuchten Störungen und tiefen Transformstörungen zusammenhängen. Der Bezug zur Sierra Leone Schwelle ist ebenfalls unbekannt. Im Zuge der SEDIS-Expedition M152/2 mit FS METEOR wurde der Lebenszyklus von Unterwasservulkanen und deren geochemischen Einfluss auf die ozeanische Lithosphäre der Bathymetrists Seeberge untersucht. Anhand der profilhaften geophysikalischer Messungen und Dredge-Proben wollen wir 1) die Wechselwirkung zwischen Krustenmächtigkeit, Tektonik und Vulkanismus verstehen, 2) die strukturelle, chronologische und petrologische Entwicklung von Vulkanen und Vulkanketten untersuchen, und 3) Auslösemechanismen, Transportprozesse und Volumina von Hangrutschungen studieren. Zur Bearbeitung der wissenschaftlichen Fragen sammelten wir mehr als 4000 km mehrkanal-reflexionsseismischer und mehr als 5000 km parametrische Sedimentecholot, Fächerlot, Schwere und Magnetik-Profile. Für die geochemischen Arbeiten sammelten wir an 14 Stationen Gesteinsproben unter Einsatz einer Dredge. Die regelmäßige Beprobung der Luft und des Oberflächenwassers diente der Bestimmung der Konzentration von heute weltweit verbotenen Pestiziden, polychlorierten Biphenylen, bromierten Flammschutzmitteln, polyzyklischen aromatischen Kohlenwasserstoffen und deren Derivaten und um den Austausch zwischen Luft und Meer weiter zu verstehen.

2 Participants

2.1 Principal Investigators

Name	Institution
Hübscher, Christian, Prof. Dr.	UHH
Augustin, Nico, Dr.	CAU/GEOMAR
Van der Zwan, Froukje, Dr.	CAU/GEOMAR

2.2 Scientific Party

Name	Discipline	Institution
Hübscher, Christian, Prof. Dr.	Geophysics, Chief Scientist	UHH
van der Zwan, Froukje, Dr.	Head Sampling	CAU/GEOMAR
Grob, Henrik	Geophysics / Shift Leader	UHH
Häcker, Tobias	Geophysics	UHH
Hartge, Matthias	Geophysics	UHH
Huster, Hendrik	Geophysics / Shift Leader	UHH
Kretzschmann, Lisett	Head Chemistry	MPI / M
Lampridou, Danai	Geophysics	NKUA
Preine, Jonas	Head Magnetics / Shift Leader	UHH
Schäfer, Wiebke	Geophysics	UHH
Schade, Martin	Head Hydroacoustics	CAU/GEOMAR
Seidel, Elisabeth	Geophysics / Interpretation	UHH
Warwel, Arne	Geophysics	UHH
Wehmeier, Lena	Geophysics	UHH
Winter, Sven	Technician (Geophysics)	UHH
Otte, Frank	Technician (Meteorology)	DWD
Raeke, Andreas	Technician (Meteorology)	DWD

2.3 Participating Institutions

CAU:	Institute for Geology / Christian Albrecht University Kiel
DWD:	Deutscher Wetterdienst, Geschäftsfeld Seeschifffahrt / Hamburg
GEOMAR:	Helmholtz Centre for Ocean Research Kiel
MPI / M:	Max Planck Institute for Chemistry, Mainz
NKUA:	Department of Geology and Geoenvironment, National and Kapodistrian University of Athens
UHH:	Institute for Geophysics / University of Hamburg

2.4 Crew

Name	Rang
Korte, Detlef Peter	Master
Apetz, Derk-Ude	Chief Mate
Graf von Keller, Magnus Tarik	2nd Mate
Mock, Benjamin	2nd Mate
Rathnow, Klaus Peter Eberhard	Doctor
Hartig, Volker Joachim	Ch/Eng.
Heitzer, Ralf	2nd Eng.
Wilhelm, Jan Erik	3rd Eng.
Schmidt, Hendrik	SET
Voigt-Wentzel, Heinz Joachim	Electron.
Schulz, Harry	2nd Electronic
Bagyura, Bernhard	Sysman
Sebastian, Frank	Fitter
Hadamek, Peter	Boatswain
O'Keefe, Darren	AB
Pleuler, Merlin Till	AB
Durst, Alexander	AB
de Moliner, Ralf	AB
Koch, Stefan	AB
Bußmann, Piotr Marek	AB
Hildebrandt, Hubert Hans	AB
Eller, Lukas	Motorman
Schroeder, Manfred	Motorman
Kudraß, Klaus Werner	Motorman
Götze, Rainer	Cook
Fröhlich, Mike Robert	Cook
Parlow, Jan	1st Steward
Shi, Wubo	2nd Steward
Zimmermann, Petra Edith	2nd Steward
Chen, Xiyong	Laundryman
Osta, Reese Patrick	Trainee
Ederleh, Tom Wilko	Apprentice
Weber, Christoph	Apprentice

3 Research Program

(C. Hübscher, F. van der Zwan, M. Schade)

3.1 Description of the Work Area

(M. Schade, F. van der Zwan, C. Hübscher)

The Bathymetrists Seamounts Chain (BSM) is situated in an area of vast morphologic diversity. Numerous transform faults and their associated tectonic lineaments intersect the eastern Atlantic plate at ~ 10° N (Fig. 3.2.1). The BSM is bounded in the north by an extension of the Vema Fracture Zone (VFZ) consisting of a "Cutting Fault" in the west, the Cape Verde Ridge (CVR) and the Guinea Fracture Zone (GFZ including Kane Gap). Those lineaments represent major topographic anomalies of the Central Eastern Atlantic basin. The VFZ with its protruding ″Cutting Fault″ reaches from the Mid-Atlantic Ridge (MAR) 2500 km to the Guinea Plateau.

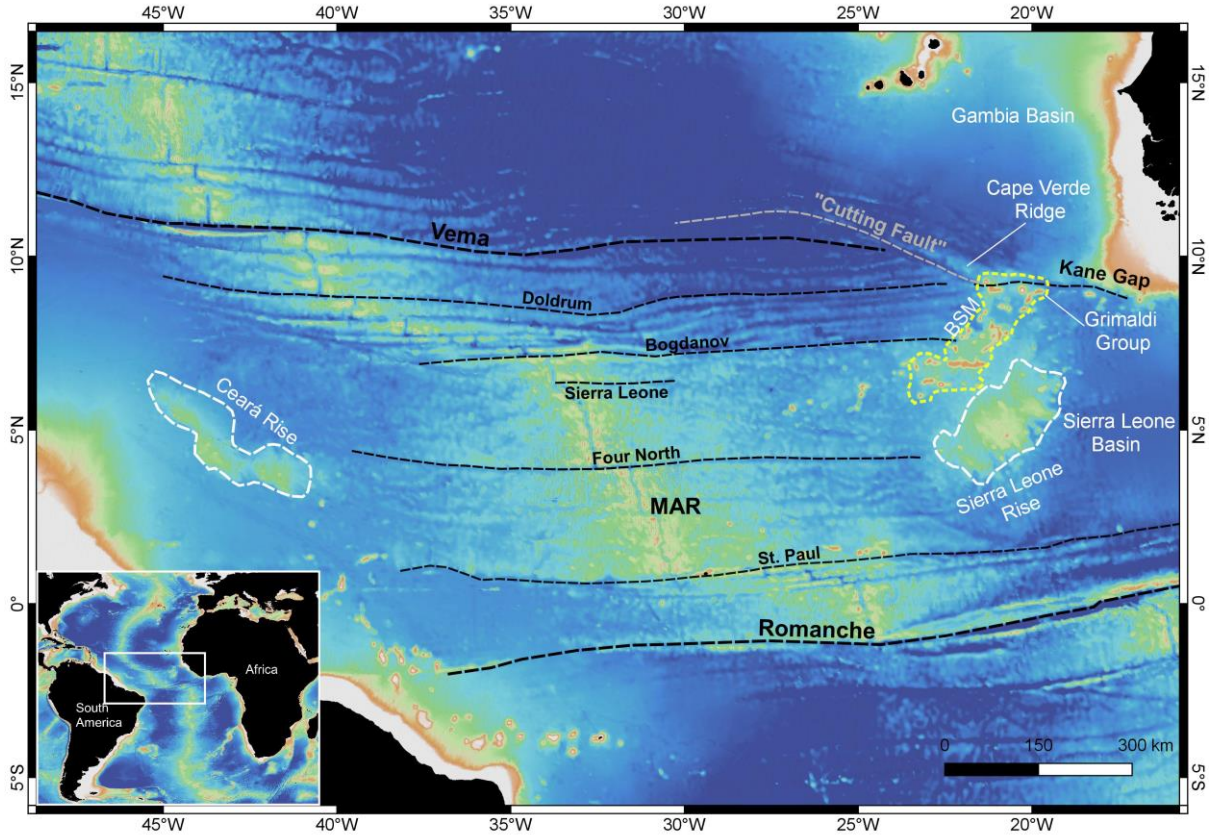

Fig. 3.1.1 Local structural overview of the Central Atlantic Ocean. Dashed black lines show main fracture zones, dashed grey line mark the location of the "Cutting Fault", a dashed white line marks the position of the Sierra Leone and the Ceará Rise, a dashed yellow line marks the BSM. MAR: Mid-Atlantic Ridge.

The SW – NE striking BSM dominate the seafloor between the Sierra Leone Basin and the Gambia Basin (van der Zwan et al., 2018). Vertical gravity gradient data (Sandwell et al., 2014) show several E – W striking lineaments south of the Cape Verde Ridge and Kane Gap which underlie the northern areas of the BSM including the Grimaldi Seamounts (van der Zwan et al., 2018). At least three neotectonic movements between the Oligocene and the Holocene formed a junction among Cape Verde Ridge, Bathymetrists Seamounts and Kane Gap, simultaneously to

the formation of the Cape Verde Ridge, second order ridges and some upwelling in the Cape Verde Basin (Skolotnev et al., 2009).

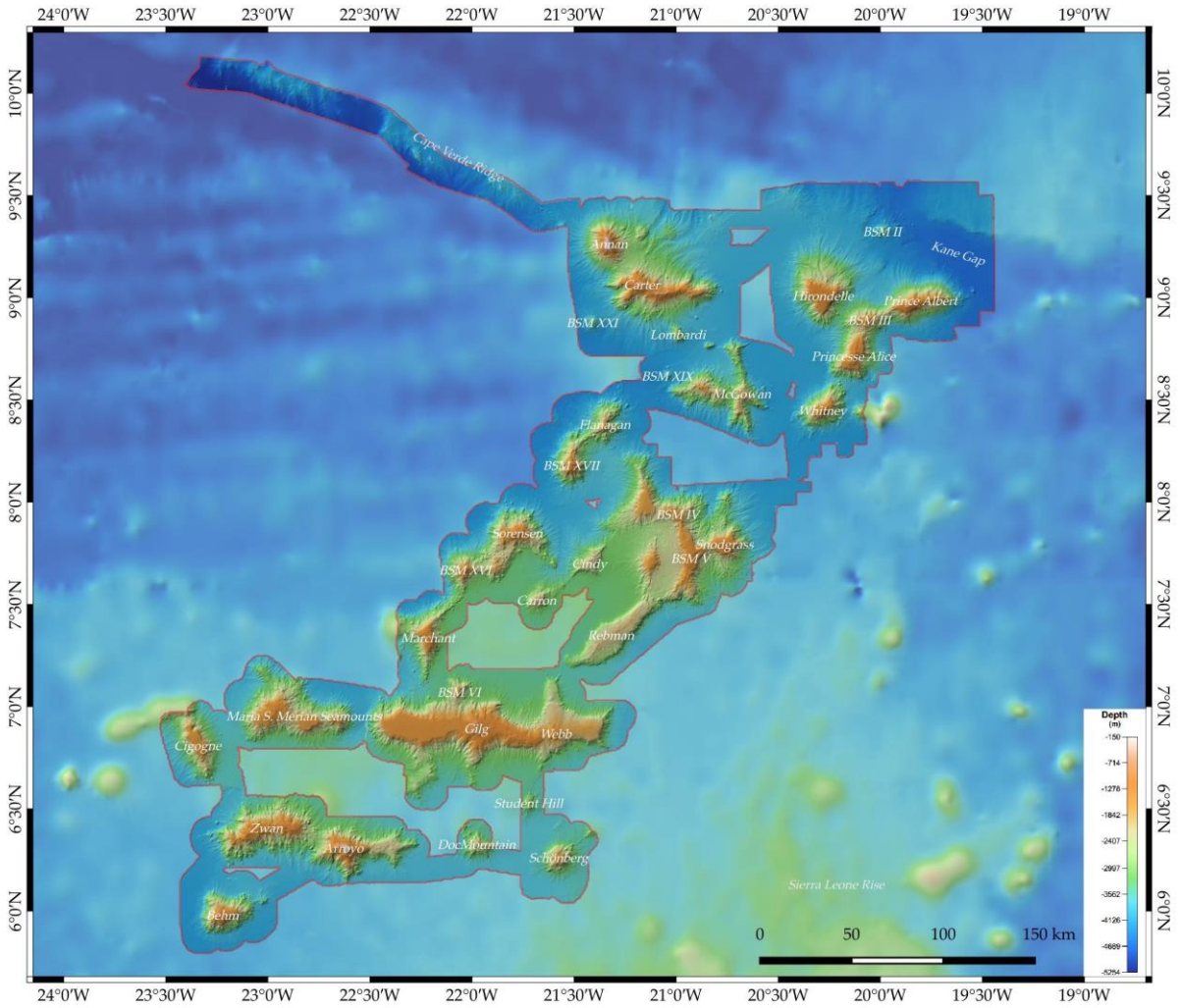

Fig. 3.1.2 Bathymetry of BSM. ETOPO bathymtry in backgroud, MSM70 multibeam data from BSM are plotted above.

The BSM has been morphologically associated with the northern part of the Sierra Leone Rise (SLR), a 600 km long and 400 km wide aseismic rise located between the Gambia and Sierra Leone Basins and separated from the African continental margin by a deep channel (Emery et al., 1975; Kumar and Embley, 1977; Jones et al., 1991). The SLR is limited by the GFZ in the north and by the St. Pauls Fracture Zone in the south. Its crest rises 2500 m above the abyssal plain in the Sierra Leone Basin (Jones et al., 2015). Bounded by the same two fracture zones, the Ceará Rise is situated west of the Mid-Atlantic Ridge. Just like the SLR, the Ceará Rise is associated with an aseismic rise and overtops the surrounding abyssal planes by about 1500 m. In contrast to the Ceará Rise the SLR is underlain by a thick igneous basement reaching a crustal thickness of 13-17 km caused by magmatic underplating (Jones et al., 2015). However, the two rises are approximately equal in area and equidistant from the Mid-Atlantic Ridge (Kumar and Embley, 1977; Fodor and Hekinian, 1981). This leads to the assumption that, based on its

distance from the Mid-Atlantic Ridge, the Ceará Rise originated together with the SLR 80 Ma ago (Kumar and Embly, 1977). During Cretaceous times, seafloor spreading in this area broke the volcanic mass into an eastern and western structure forming both rises (Kumar and Embley 1977; Fodor and Hikinian, 1981). In addition, the magmatism of the Bathymetrists Seamounts has been suggested to be connected to the SLR (Kharin, 1988; Emelyanov et al., 1990) but it remains unclear if that is actually the case due to limited samples of the volcanic basement and limited ages of these.

In addition to the complicated tectonic setting and its relation to the SLR, little is known about the origin, age and nature of the Bathymetrists Seamounts. Two hypotheses have been proposed for the origin and formation of the Bathymetrists in the late Paleocene, which are (a) the rising of a deep mantle plume, possibly by bending or a detached offshoot of the Sierra Leone plume (Peyve and Skolotnev, 2009), where the spatial positioning of the two seamount chains was determined by local plate tectonics (e.g., Schilling et al., 1994; Peyve, 2011; Skolotnev et al., 2017), or (b) decompressional melting of asthenosphere mafic rocks due to extension along the Guinea FZ (Jones et al., 1991; Skolotnev et al., 2012), with each process having its own effect on the oceanic lithosphere.

RV MARIA S. MERIAN cruise MSM70 took place at the BSM (van der Zwan et al., 2018) That expedition aimed at characterizing the structure, age and composition of the Bathymetrists Seamounts and adjacent areas to understand their origin and formation mechanism, which will allow a better assessment of how intraplate volcanism modifies the structure and composition of oceanic lithosphere through time. During that cruise the bathymetry of the Bathymetrists Seamounts and adjacent areas has been mapped with the hull-mounted multibeam system (Fig. 3.1.2). A total of 65 dredge-tows recovered volcanic samples, carbonates, phosphorites, mudstones and manganese crusts and nodules from 27 seamounts.

The new high-resolution bathymetry shows that most of the seamounts have steep slopes with erosional channels and (62%) resemble flat-topped seamounts or guyots capped by carbonated platforms, manganese-iron or phosphorite crusts as has been observed in the Pacific (Hess, 1946). Most of the seamounts have a top at 1000 m depths, but some are as shallow as 200-300 m depth. The abundant presence of landslides all around the volcanoes indicate extensive flank collapses and erosion of the volcanoes. The bathymetry of the seamounts shows three prominent main axis orientations. One axis lies parallel to the fracture zones (E – W striking) and is more common in the southern part of the BSM Chain. The second type of axis can only be found in the northern part and lies oblique to the fracture zones, which lead to a NE – SW striking of the seamounts. The third main orientation is parallel to the ridge axis. The morphology of the seamounts indicate a clear structural control for volcano formation, potentially related to the local fault patterns and re-organization of the African plate movement. With the current information it can however not be determined if these faults caused decompression volcanism, or merely controlled the pathway of upcoming melts. Samples from the volcano flanks reveal dense basaltic samples and vesicular volcanoclastic breccias of mafic origin containing pyroxenes, amphiboles and biotite. The last type of samples could either be the result of flank collapses that are observed in the bathymetry or an intrinsic characteristic of the volcanic eruptions (e.g. high volatile contents).

3.2 Aims of the Cruise

(C. Hübscher, F. van de Zwan)

The RV METEOR cruise M152/2 strived for a better understanding of the life cycle of submarine volcanoes and their effect on the oceanic lithosphere in the oceanic intraplate setting of the BSM (Figs. 3.1.1-2). We intended to

1) understand the interaction between crustal thickness, tectonics and volcanic phases,
2) investigate the chronological evolution of individual seamounts and seamount chains,
3) study the structural growth process of elongated seamounts,
4) review slope failures and resulting mass flow processes.

We addressed these objectives by high-resolution reflection seismic, parametric echosounder (Parasound), multibeam, gravity and magnetic profiling as well as by rock sampling.

3.2.1 Interaction Between Crustal Thickness, Tectonics and Volcanic Phases

Expedition MSM70 (van der Zwan et al., 2018) showed that the volcanoes of the BSM show strong lineations, which indicate a structural control for magma ascension. It seems obvious that the northern and southern W-E striking seamount chains emerged along fracture zones that cross the BSM in the same direction. However, the nature of the NE-SW striking chains remains unclear. In case magma ascends along tectonic faults, we expected that the seismic data elucidate whether the seamounts emerged above normal/listric, strike-slip or transtensional faults.

Although faults clearly play a role in the position of the extruded melts, the origin of these melts is debated. The steep and high flanks of both Guinea and St. Pauls fracture zone may imply that the fracture zones disturb the ocean floor to great depths which would facilitate the concept of deep decompressional melt in fracture zones, expressed as alkalibasalts (Melson, 1967) as also found at the BSM. Drifting of the oceanic crust over a mantle plume could explain the overall NE-SW trend of the seamounts, but implies a progressive age relationship, which currently cannot be evaluated due to very limited age data.

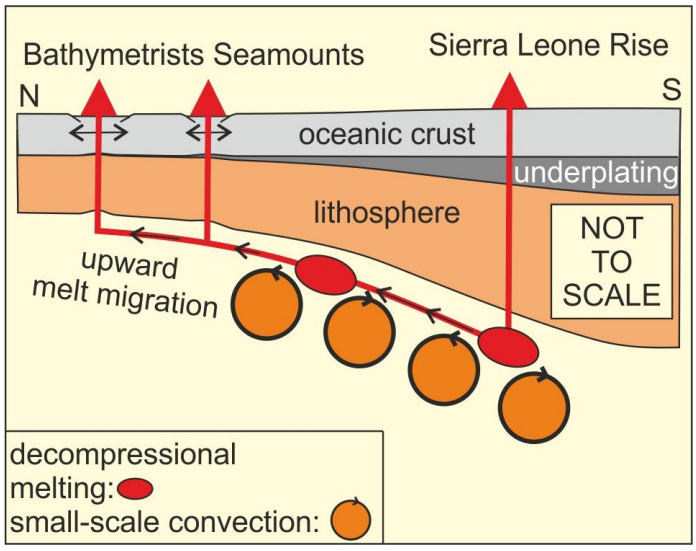

Fig. 3.2.2 Working hypothesis: small-scale sub-lithospheric convection (SSC) beneath the Sierra Leone Rise drives volcanism beneath the Bathymetrists Seamounts.

Based on the recent MSM70 expedition, another mechanism for intraplate volcanism without a linear age-relation-ship has been hypothesized by Schade (2018), which adapts a model of small-scale sublithospheric convection (SSC) by Ballmer et al. (2007). Small-scale sublithospheric convection as melting mechanism to form intraplate volcanic provinces as alternative to plume volcanism, has been earlier suggested for e.g. the Cameroon Volcanic Line (King and Ritsema, 2000; Reusch et al., 2010) and for

the Fernando de Noronha volcanic province (Knesel et al., 2011). According to this hypothesis, intraplate volcanism at the Bathymetrists Seamounts (BSM) is driven by small-scale sub-lithospheric convection (SSC) that started beneath the SLR (Fig. 3.2.1). Plume-ridge interaction during the early evolutionary phases of the SLR caused magmatic underplating which increased the crustal thickness of the SLR to 17 km (Jones et al., 2015). SSC could be the effect of a difference in lithospheric thickness between the BSM and the SLR, causing edge convection transporting melts from beneath the SLR towards the BSM. Alternatively, such a convection spontaneously occurs if the cold thermal boundary layer (TBL) below oceanic lithosphere surpasses a threshold thickness (Ballmer et al., 2009). Underneath the thickened lithosphere SSC organizes as rolls aligned with plate motion and parallel upwelling areas spaced 200-300 km (Richter and Parsons, 1975, Ballmer et al., 2009). Potential deep decompressional melting may occur within the upwelling areas and melts, migrating along the Moho, may breaches the crust is if this is weakened by tectonics. If the plate underlies changes in its motion, fracture zones are exposed to extensional and compressional stress (Bonatti, 1977). Times of extended stress can weaken the oceanic crust along those lineaments and serve as a valve of rising magma, which finally leads to volcanism. Here, the BSM developed. Possibly, seafloor volcanism on the SLR was also reactivated.

3.2.2 Chronological Evolution of Seamounts

If the BSM chains formed by drifting of oceanic crust over a magma source like a mantle plume, the individual seamounts should show an age progression. In case of SSC-driven volcanism one would expect a non-linear relationship between individual seamounts of the two NE-SW striking seamount chains. The ages of the individual samples collected during MSM70 will represent one chain of arguments to unravel the chronology of the BSM evolution.

However, the ages that can be obtained from sampling are limited, considering the huge area and in all cases each of the seamounts developed over a longer time period of active volcanism. Different ages of samples do not necessarily completely resolve the order of seamount evolution, since a sample from one seamount might represent an early phase, while a sample from an adjacent seamount may reflect a late stage. Imaging the onlap-pattern of lava flows from adjacent seamounts will provide insight into the synchronous or asynchronous evolution of the seamounts and seamount chains. Additional sampling by dredging of the SLR will allow constraining the age relationship between BSM and SLR.

3.2.3 Structural Growth process of Elongated Seamounts

There are different models on how large intraplate seamounts are formed. So far unpublished seismic data from the Azores show that intraplate seamounts away from the Terceira Rift start to develop as single volcanic cones (Stakemann, 2016). Adjacent eruption lead to a stacking pattern of cones which later transform to elongated ridges. The 2nd endmember model is that the seamounts formed by fissure eruptions, which may be relevant for the BSM if they are controlled by faults. Seismic data will show the internal structure of the seamounts and how they were formed. Contrary to the Azores, the crests of the guyot like seamounts of the BSM are eroded, thus we will study both the eroded elongated seamounts (e.g. Carter Seamount, Gilg and Webb Seamount) and deeper, less eroded seamounts for this purpose. The seismic data to be collected during the here proposed survey will further elucidate the nature of the vast of rather circular

mounds having a diameter of about 1 km. These features represent either parasitic flank eruptions as observed at Sao Migues (Azores; Weiß et al., 2015b) or slided blocks (debris).

3.2.4 Trigger Mechanisms, Transport Processes and Volumes of Slope Failures

In high-resolution bathymetry many slope failures can be observed on the BSM (van der Zwan et al., 2018). There is no obvious correlation between the location of slope failures and the inferred location of tectonic faults along the summits of the individual seamount (for an instance see Fig. 3.4). One might speculate that the slope failures result from earthquake triggered gravity collapse, but the seismic data will show if secondary faults beneath are present.

The reflection seismic data will show insights in the destruction processes of intraplate seamounts and allow concluding on the transport mechanisms (slumping, sliding or turbidity currents). These data are further needed to distinguish between slided blocks and volcanic cones.

3.3 Agenda of the Cruise

(C. Hübscher)

3.3.1 Profile and Station Map

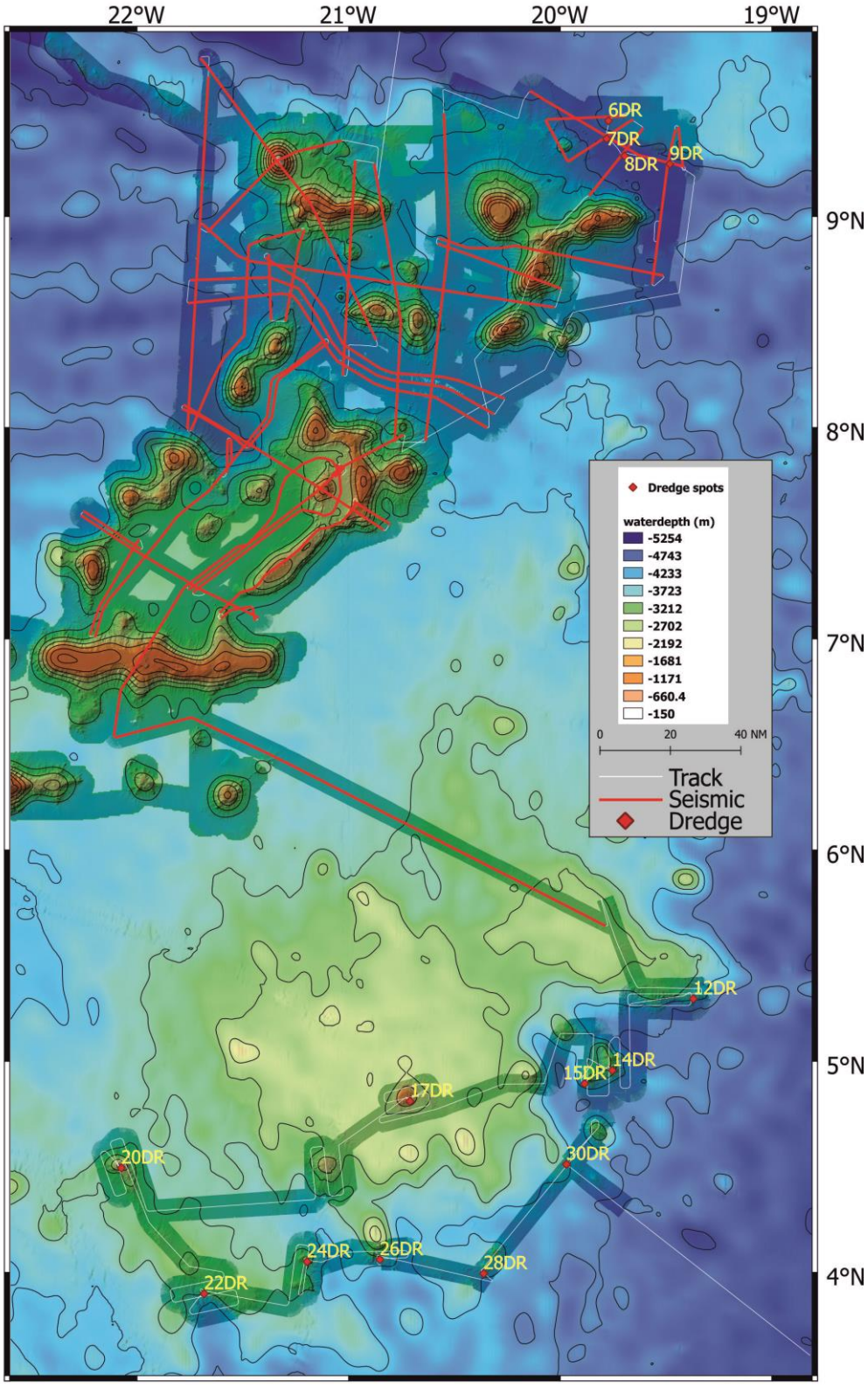

Fig. 3.3.1.1 Map (ETOPO and MSM70/M152/2 multibeam) with M152/2 track (white line), seismic profile (red line) and dredge (diamond) locations.

3.3.2 Deviations From the Original Work plan

RV METEOR cruise M152/2 has been accomplished without any problems. The geophysical profiles had been significantly adapted due to underway findings. Seismic data acquired during the first week across the summits or along the crests of the seamounts revealed little signal penetration and brought very limited scientific value except for magnetic data. Consequently, we designed profiles between the seamounts and in prolongation of the seamount lineations with the aim to image presumed underlying faults. The entire sediment packages in the BSM area is characterized by Y-shaped or listric blind faults, preliminary interpreted as polygonal fault systems (PFS), which superimpose plate tectonic driven faults. In order to distinguish between both fault mechanisms we will have to carry out a fault displacement analysis later on. A crucial prerequisite will be the presence of narrow spaced parallel profiles, which took time to collect. Without the collected dense seismic profiles no reliable interpretation will be possible. We therefore focused on the northern and central BSM and limited the geophysical profiling at the SLR except for one profile which ties the BSM profiles with DSDP Leg 42, Site 366 at the SLR. Based on underway findings we further developed a working hypothesis regarding environmental processes that controlled the development and evolution of rather unusual manganese nodule accumulations found during MSM70. In order to test this hypothesis we carried out an additional 18 hour dredge program at Kane Gap. We saved this time later by increasing speed over ground during seismic profiling when surface currents came from the aft, allowing higher speed over ground by relative lower speed through water.

3.3.3 Measures of Responsible Conduct of Marine Research

The scientific work performed during Expedition M152/2 strictly adhered to the “Maßnahmen im Hinblick auf die Erklärung zu einer verantwortungsvollen Meeresforschung” and the Code of Conduct for Responsible Marine Research in the Deep Seas and High Seas of the OSPAR Maritime Area.

Mitigation measures for the operation of seismic and hydroacoustic sources with pulsed sound emissions were as followed. Before a source was first triggered, always during daylight, we scanned the area around the vessel up to a distance of 500 m (mitigation radius) for marine mammals (MM) from the bridge for 60 minutes. Measurements only commence if no MM were observed within the mitigation radius. The study area is not known as a breeding and nursery areas of MMs. Short interruptions did not happen, since we continuously collected seismic data also during profile changes in order to get the stratigraphic tie. Measurements started with a soft start over 20-30 minutes.

Sampling and acoustic measurements were restricted solely to methods and areas being essential to conduct the research outlined above, and the number of sampling stations has been reduced to the necessary minimum. Careful selection of sites for hard rock sampling by dredging allowed us to carry out short dredge tracks (<700 m in length), to minimize the number of dredges and the impact of dredging to the marine habitat.

There was no duplication of previous studies, since little samples exist from the vast majority of the proposed study areas thus far and the locations of known samples and seismic data were verified before scientific operations.

4 Narrative of the Cruise

(C. Hübscher, F. van der Zwan)

The scientific party arrived at RV METEOR in Las Palmas (Gran Canaria, Spain) on Wednesday, January 2nd, 2019 in the afternoon. Instantaneously we started with unloading the equipment from the containers and the installation on deck and in the labs with great support by Master Detlef Korte and his crew. After gravity tight measurements next morning in the harbour, the sea gravimeter was calibrated. Simultaneously, equipment installation proceeded and at 12:30 all scientific resorts reported ready to sail status. At 13:00 RV METEOR put to sea on schedule on a southbound track. We left the EEZ of the Cape Verdes on January 6 at 18:10 UTC and switched on the multi-beam for bathymetric and the acoustic Doppler current profiler (ADCP) for current-depth measurements. We further started water and air sampling.

The transit to our working area north of the Sierra Leone Rise (SLR), where volcano lineaments form the Bathymetrists Seamounts (BSM), lasted until January 7th in the morning. The 5 days of transit had been used for training the deck handling of the heavy gear and for educating younger scientists in the duties during the shifts. After arrival at the north-western tip of the BSM we deployed the digital streamer system, which lasted 2 hours because seven digitizer modules had to be installed in the streamer. After that we brought out the magnetometer (gradiometer). During the installation an observer carefully watched out for marine mammals. Since no mammals were spotted we deployed the seismic sources and started to ramp up the pressure during 30 minutes. The procedure of mammal observation and ramp up was repeated throughout the cruise after each seismic shut down. After synchronizing the sources we started regular geophysical profiling at 18:30 ship time, which included multi-channel seismics, parametric echo-sounding (PARASOUND), multi-beam (Kongsberg EM122), gravity and magnetic measurements. With the first profile we crossed the Annan volcano, a real giant being more than 60 km wide and 6 km high, with a base more than one kilometre beneath sea floor. A carbonate platform had developed on Annans top that is today in a water depth of ca. 200 m. Next morning on the 8th we started a profile west of the seamounts and across a fracture zone. We learned that Annan developed on the southern shoulder of the previously crossed fracture zone. A 2nd, cross-profile over Annan and other seamounts to the south taught us that profiles across the summits of the seamount provide just minor insight into their internal structure and possible underlying faults. Consequently, we designed the profile layout in a way that profiles cross either the lower seamount slopes or lay in between the seamounts. Around noon on the 9th we did some maintenance on the seismic source system and recommenced surveying after three hours. Until January 11th in the morning we collected more profiles perpendicular to the presumed striking directions of underlying faults and fracture zones in the northern BSM area. Same day we collected a profile along the Guinea Fracture Zone, passing Kane Gap where the fracture zone narrows. Here, the Kiel group had dredged an interesting accumulation of manganese nodules one year before in the course of RV MARIA S. MERIAN cruise MSM70. With profiles across the fracture zone we strived for investigating those processes that controlled nodule accumulations, which lasted until the 12th late evening. The next two days we focussed on investigating possible faults that strike north-south, so we collected mainly west-east profiles which will help us later on to link the stratigraphy between the previously collected north-south going lines. January 14th we selected profiles for two days that linked the lower slopes of various

seamounts, which are telling us about the relative order in which seamounts evolved. We used the following two days until January 16th for collecting three relatively closely spaced profiles along strike the non-volcanic area that separates the northern from the central seamount group. In the morning of January 18th we brought all gear on deck.

Based on the processing results we decided to continue our measurements around Kane Gap, so we travelled a fast transit of 10 hours, during which we did a close inspections and regular maintenance of all towed equipment. In the afternoon the same day, we deployed the equipment again and commenced profiling in the Kane Gap area. On the 19th before noon, the equipment was put on deck again. During the next ca. 18 hours four dredges were taken in order to test hypotheses about those processes that control manganese nodule growth. Two dredges included several nodules, one was empty as expected, and one was unexpectedly empty.

From noon on we transited on a southbound track to the central BSM where we arrived in the afternoon of January 20th. After deployment of the seismic and magnetic gear we started a profile along strike and in between the northeast-southwest striking volcano chains of the central BSM, in order to map faults that laterally offset the volcano chains. Next day we started measurements along a set of profiles which targeted on investigations the eastern Rebmann volcano, which lasted until January 22nd. During the following 24 hours profiles perpendicular to the strike of the volcano chains were taken in order to better understand possible fault systems that underlie the volcano lineaments. Along strike profiles measured from 22nd to 23rd imaged the syn- and post-volcanic sediments between the western and eastern volcano lineaments, followed by profiles in the transition zone between the southwest-northeast striking central BSM domain and the west-east striking southern domain. January 24th to 25th we collected profiles parallel and in close distance along-strike and within the central BSM, which will enable us to correctly identify individual faults systems imaged in the individual profiles. In the night from 25th to 26th we crossed the W-E striking and about 140 km long Webb-Gilg volcanic ridge. With the last profile, having a length of almost 300 km, we connected the southern BSM with DSDP Leg 41 Site 366 at the south-eastern SLR, where we arrived on January 27th in the morning. Here, the seismic and magnetic survey ceased, and at noon all towed gear was safely on deck.

For the following five days we investigated the SLR with multi-beam and dredge sampling. We chose those areas which showed on the low-resolution GEBCO bathymetry the most relief, which are only present on the south side. From the detailed multi-beam pre-site surveys we then determined locations which revealed high backscatter amplitudes (meaning hard ground) and slope gradients of > 20°. On the 27th and 28th three dredges were taken on the south-eastern collapsed flank of the main plateau, at depths of 3000-4000 m. Two dredges included volcanic rock, one was empty. We dredged several potential volcanic cones on the rise from east to west and at a depth of ca. 2000 m on the 29th and 30th. The dredges returned carbonates, so we focused again on the deeper flanks of the plateau moving back towards the east. Two dredges caught chemically modified carbonates (phosphorite) in 3000 m water depth. One of the last dredges on February 1st returned volcanic samples from 3800 m water depth.

The scheduled station program ended around noon and RV METEOR immediately started the south-east bound transit with just the gravimeter, multi-beam and air and water sampler left active. Same evening, Triton showed up and announced equator baptism for the next day. The transit to the Namibian EEZ lasted until February 10, where multi-beam, air and water sampler

were switched off. During this time, final data processing on board and rock descriptions were performed, as well as the packing of the equipment. The cruise finished on February 11, when RV METEOR completed her transit and berthed at Walvis Bay harbour.

5 Preliminary Results

(C. Hübscher, F.M. van der Zwan and Scientific Party)

5.1 Equipment

5.1.1 Multi-Channel Seismics

(H. Grob, H. Huster, J. Preine, S. Winter, C. Hübscher)

The seismic signals were generated by means of an array of two GI-Guns towed in a depth of approx. 3.5 m behind the ship's stern. For the first three profiles one GI-Gun was operated in 'true GI mode' with corresponding air volumes of 45 cin for the generator and 105 cin for the injector. The second GI-Gun was operated in 'harmonic mode' with a 105 cin generator volume and 105 cin injector volume. For the subsequent profiles both GI-Guns were operated in 'harmonic mode' with chamber volumes of each 105 cin. The SureShot trigger system synchronized both GI-Guns and displayed the source signal of each airgun. The firing time interval amounted to 10 s. Expendable Sound Velocity Probe

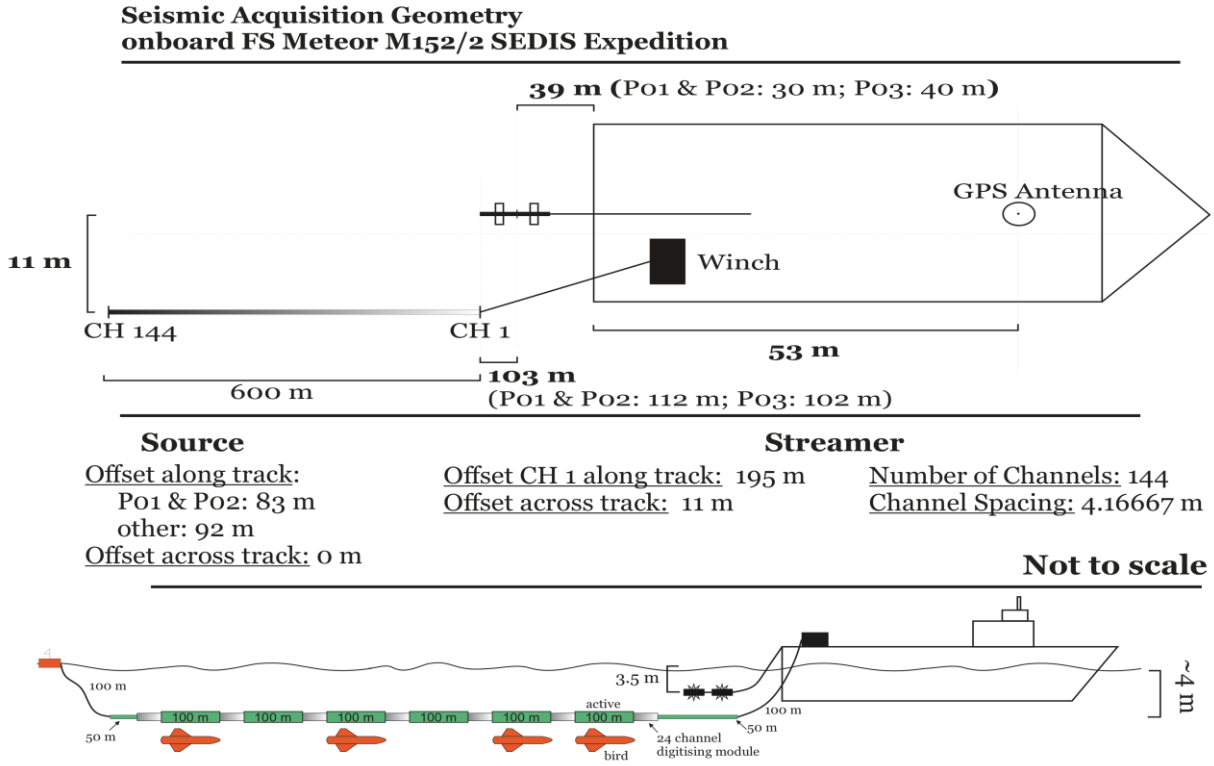

Fig. 5.1.1.1 Scheme of multi-channel seismic acquisition

The digital streamer used for the survey was a Hydroscience Technologies SeaMUX 144-channel array with an active length of 600 m having a symmetric group interval (Fig. 5.1.1.1). The streamer data were digitized by seven SeaMUX 24 channel 24 bit digitizing modules. These modules were configured in six multiple arrays totalling 144 channels. Both the digitizing modules and the data acquisition hardware are bi-directional, allowing operation from either end of the array. The modules were powered via a 1.2A DC constant current loop which allowed for

the use of small gauge wires, reducing the size of the wire bundle. The 24 analog inputs of each module were sampled at 1 ms via 24 bit delta sigma converters. Recording length was 8 s for the first two seismic lines and 9 s for the remaining lines. Digitized data (along with data from modules behind the unit) were sent to the recording system via a telemetry system made up of twisted wire pairs. Four Concord Navigator birds were used to keep the streamer cable at the desired depth of 4 m. The high-resolution seismic data acquisition was done using a Hydroscience Technologies SeaMUX recording system. The Navigator birds were controlled by an extra PC. Data were stored in SEG-Y format.

All seismic lines were processed on board with the 2016 VISTA® desktop seismic data processing software by Schlumberger. Following processing steps were applied:
1.) Bandpass filtering, 2.) trace editing, 3.) forward and backward tau-p transformation for denoising, 4.) scaling and gaining, 5.) velocity analysis and NMO correction, 6.) Finite-Differences migration, 7.) 4D-Dec white noise suppression and 8.) final scaling.
Final processed seismic lines were subsequently imported to the IHS Markit Kingdom™ (version 2016) interpretation software and were ready for on board interpretation.

5.1.2 Dredge Operations Measurements

(F.M. van der Zwan, M. Schade)

Ground truething of and rock sampling was performed by the towing of a large Chainbag Dredge. Dredge locations were selected based on high-resolution multibeam data. For dredges aiming to collect volcanic samples, tracks were planned on areas with high backscatter reflection (indicating hard seafloor) and a steeper slope.

The dredge was lowered to the seafloor at the beginning of the track and while the ship moved to the end position on the dredge track, we laid out more cable. Subsequently, the dredge was towed over the seafloor collecting hard rock samples. Sediment traps in the corner of the dredge collected sediments associated with the hard rocks. Dredge tracks were kept with 200-690 m, short to limit seafloor impact.

We deployed 14 dredges during a total of 41 hours and 13 min. in Kane Gap and at the Sierra Leone Rise. At Kane Gap water depths were between 4890 and 4270 m onto slopes between 0° and 5°. At the Sierra Leone Rise we cast dredge tows at slopes of 20-45° in water depths of 4230 to 1750 m. On average a dredge tow took 2 hours and 57 min.

5.1.3 Multibeam Measurements

(M. Schade, D. Lampridou)

During Meteor expedition M152/2, a bathymetric dataset of approximately 48,229 km^2 of the equatorial Atlantic Ocean between 09.812°N to 03.750°N and -22.321°E and -19.250°E was collected including the Bathymetrists Seamount Chain, the Kane Gap, the Central Sierra Leone Rise as well as the south-eastern flank of the Sierra Leone Rise Fig.

Multibeam and backscatter data were acquired using the hull-mounted Kongsberg EM122 12kHz echo-sounder. The EM122 multibeam collects bathymetric, corrected backscatter and water column imaging (WCI) deep water data via a wide swath with maximum excess of 150 degrees (2 x 75°). The installed configuration on board of RV Meteor operates with a frequency of 12 kHz at water depth of up to 11000 m. It has an across-ship swath width of up to 6 times the depth to approximately 30 km with 432 soundings per swath. Data was collected at variable ping

rates depending on water depth with a ship speed of 5 kn during the multichannel seismic surveys in the area of the BSM. During the mapping operations at the SLR the ships speed was increased to 10-11 kn. The survey speed at the Sierra Leone Rise was relatively high for mapping but required to cover the survey area properly in the available working days. Transit data were recorded at >12 knots and greater water depths (>4,000 m) and result in grids with a resolution of 100 m per cell (Backscatter 50 m) and will be part of the AtlantOS project. Beam widths were normally kept between 60° and 65° in typical water depths of 3,500 – 1,000 m, but occasionally increased to 70° in shallower water. In addition, the EM122 is equipped with a function to reduce the transmission power to avoid hurting mammals if they are close by.

Data acquisition was conducted via the Kongsberg Seafloor Information System (SIS) Version 4.3.2, running in a Microsoft Windows 7 environment.

Three XBT measurements were performed within the working area to measure sound velocity profiles, that were used to correct the hydroacoustic signals. Obtained sound velocities were compared to the those of expedition MSM70 (Fig. 5.1.3.1). Due to a better resolution of the XSV/CTD generated sound velocity profiles and only marginal differences of the different SVP's in the few uppermost meters of the water column, the CTD SVP of expedition MSM70 was used to gain a constant corrected bathymetric survey of the working area and avoid refraction artifacts. The bathymetric record was edited directly after its collection. The data editing was made with Qimera (QPS Software) including an 3D-Editor with an outlier's tool to filter overhanging and underlying pings. Further editing was done manually within the 3D-Editor and 2D-Slice Editor. The final edits were exported as an .xyz file for gridding the bathymetric record using the Fledermaus™ module. Backscatter data, providing information about the reflectivity of the seafloor, were visualized using FMGT (QPS Software). A 3σ filter was applied in FMGT to the backscatter data to emphasize the difference between higher and lower backscattering areas. All the collected data has received a full post-processing and do not require further editing on shore. Thus, the bathymetric data are fully available for research directly after the cruise.

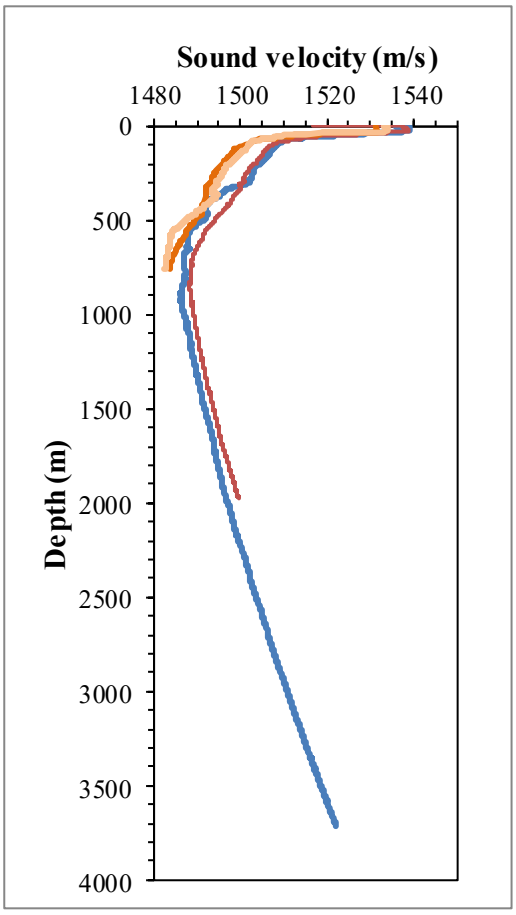

Fig. 5.1.3.1 Comparison of the MSM70 sound velocity profiles (blue, orange) and two of the M152/2 profiles

5.1.4 PARASOUND

(C. Hübscher, H. Grob, H. Huster, M. Schade, L. Wehmeier)

The hull mounted PARASOUND system sediment echosounder (Atlas Hydrographics) represents a narrow beam sediment sub-bottom profiler. Two frequencies (18 kHz and 22 kHz)

are emitted from hull-mounted transducers. Due to the parametric effect a 4 kHz signal is generated in the water column within an emitting cone of ca. 4°, which results in a foot print with a diameter of 7% of the water depth.

The signal penetration depth strongly depends on the lithology, grain size and gas load. The received data are digitised and stored in SEG-Y and PS3 format. Data processing included navigation processing (conversion of altitude and longitude into UTM Zone 27 coordinates), trace binning (12 m) and stacking, bandpass filter and gain. For interpretation we uploaded data into the Kingdom™ interpretation system.

5.1.5 Magnetic Measurements

(J. Preine)

The magnetic data collected during M152/2 SEDIS cruise were acquired using a proton precession SeaSPY longitudinal gradiometer configuration. Two magnetometers were towed in a distance of approx. 300 m behind the vessel. The cable used to tow the magnetometers was deployed from a winch. The recording station was set up in the seismic lab and acquisition was performed using the BOB software. Figure 5.1.5.1 shows the geometry of the magnetic acquisition.

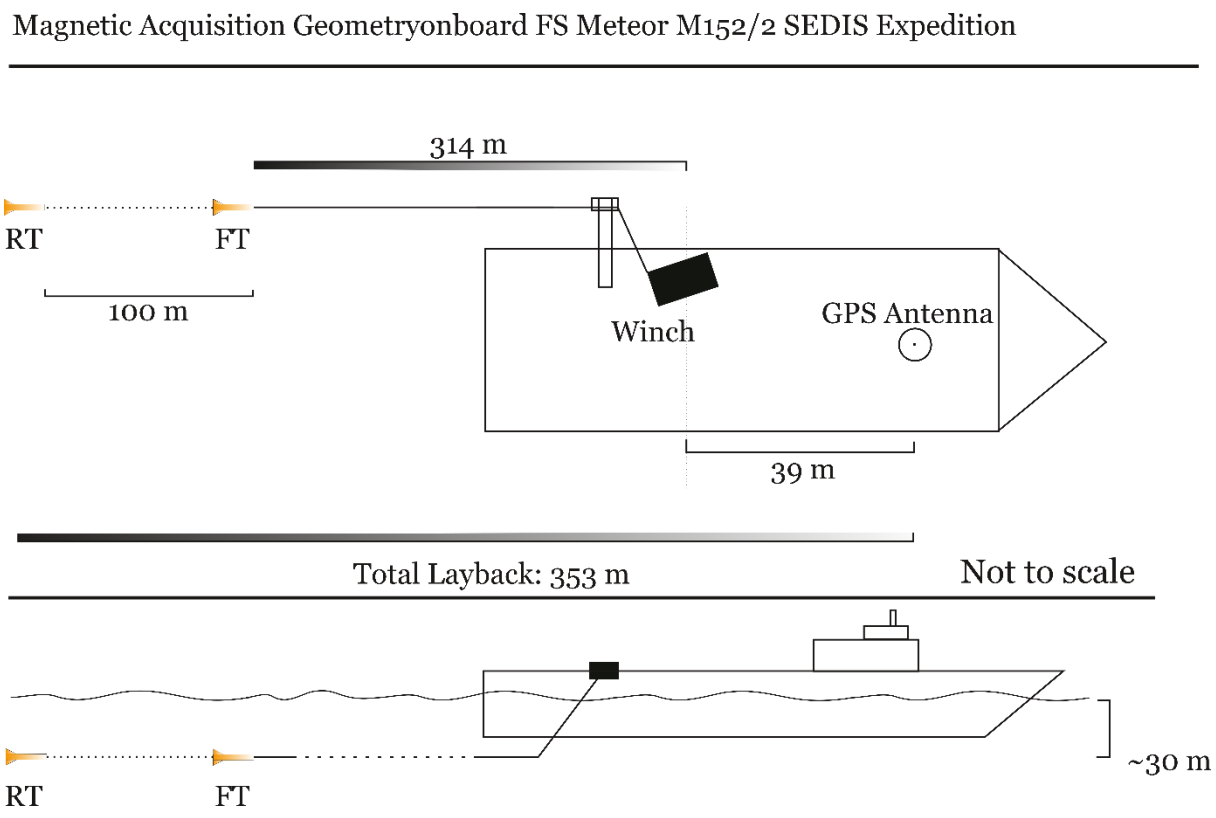

Fig. 5.1.4.1 Geometry of the magnetic acquisition.

The SeaSPY sensors are high sensitivity total field magnetometers packaged in a rugged marine housing. The measurement of the magnetic field is done inside the towed fish, while the tow cable supplied power to the towfish and a bi-directional digital communication link. The main sensor of the system is an *Overhauser total field sensor*. It operates on the proton spin resonance principle. A proton-rich liquid within the sensor is engineered in a way to allow a principle

known as the Overhauser effect to occur within it. The sensor measures the magnetic flux density, which is measured in Tesla [T].

The flux density on the surface on the Earth typically varies between 18 µT and 70 µT. It varies on any fixed location due to large scale variations e.g. from the sun or the earth's molten interior. The magnetic flux density is related to the total magnetic field by the surrounding material with different magnetic permeability. Some materials will distort the surrounding magnetic flux density. This relation can give valuable information about geological processes. In order to neglect the large-scale variation of the magnetic field, we used two magnetometers that were towed behind each other. By subtracting the measured values from each other, the gradient is calculated which should not be affected by large-scale variations. The distance between both magnetometers was 100 m. The distances of the sensors from the ship were more than the recommended minimum distance (some 270 meters for the length of RV Meteor). For this reason, the quality of magnetic data recorded was very good. The towing depth can be controlled with the speed of the vessel, which resulted in a towing depth of approx. 30 m (see figure 5.1.4.1). During our measurements the speed of the vessel was kept between 5 and 8 kn. The sampling rate was set to 0.2 Hz. The positions as well as the measured values were displayed in real-time on the acquisition software.

5.1.6 Gravimeter

(C. Hübscher)

The high performance Gravity Meter System KSS31M was operated throughout the entire cruise. It consists of the KT 31M gyro-stabilization platform, the GSS 31M gravity sensor and a data handling subsystem.

The sea gravity system is divided into three sub-systems:

- Gravity sensor GSS 31M
- Gyro-stabilized platform KT31M
- Data handling and control system ZEK 31M

The characteristics and functions of the individual building blocks are:

Gravity sensor

- Vertical non-astatized tube shaped mass
- Non-sensitivity in horizontal direction
- Temperature stabilization, pressure tight and magnetic shield housing
- Ball calibration device
- Electrical damping of superposed vertical accelerations
- Detection of gravity changes by an electromagnetic system
- Analogue/pulse rate conversion of the sensor output
- Range: 10.000 mgal
- Instrument drift < 3 mgal/month

Gyro-stabilized platform

- Electrically erected vertical gyros
- Continuous gyro erection control
- Continuous compensation for earth rotation, ship's speed, accelerations, heading errors

Control systems

- Reduction of amplitudes of accelerations caused by sea motion
- Data exchange with external navigation
- Gyro erection control and compensation of acceleration
- Overall system control
- Internal test routines

The dockside calibration of the sea gravimeter is necessary in order to tie survey data to the World Gravity Net and to combine different data sets by means of a common base. This calibration was performed using a G260 LaCoste & Romberg land gravimeter.

5.1.7 Water and Air Sampling

(L. Kretzschmann)

In order to determine persistent organic pollutants (POPs) in surface seawater and air of the equatorial Atlantic and to characterize the chemical composition of air masses going into the trans-Atlantic transport to the Caribbean (trade wind zone) air and water samples were taken during R/V Meteor expedition M152/2.

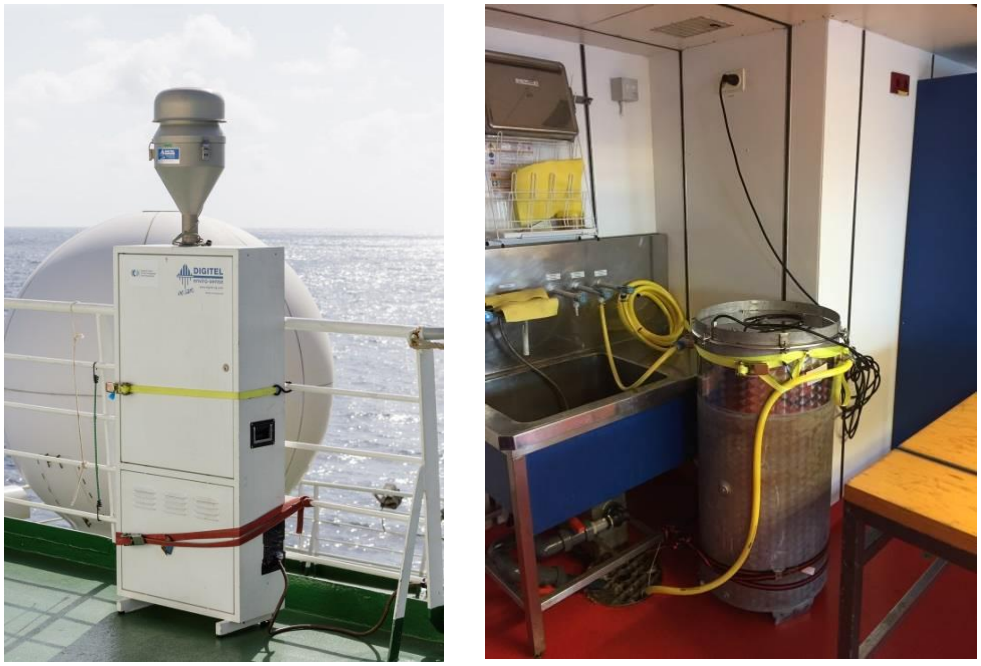

Figure 5.1.7.1 a) High-volume air sampler DH-77 at the 3rd superstructure deck. b) 200L barrel for seawater sampling.

Air samples were collected by using a high-volume air sampler DH-77 (Digitel, Switzerland) equipped with a PM10 sampling head (Figure 5.1.7.1a). The Digitel was positioned in the front part of the ship, directly under the bridge at the 3rd superstructure deck, 12.9m above the water surface.

For sampling a clean workspace in an under-deck laboratory was prepared with aluminium foil every time before changing filters. Tweezers and the trays for filters were cleaned with ethanol. A quartz microfibre filter QMA (Whatman, United Kingdom) and 2 sequential polyurethane foam (PUF) plugs were prepared and transported to the device by using aluminium foil and additionally stored in a clean zip-lock to avoid contamination. Air filters were changed

daily after 1400min of sampling. QMA and PUFs were wrapped separately twice in aluminium foil and stored in a zip-lock at -20°C.

For seawater sampling a passive sampler system was installed in the wet lab. The 200L-barrel was fixed to the wall and connected to the seawater tap (Figure 5.1.7.1b). Unfiltered Seawater was taken from the bulbous bow of the ship 4m below the surface and pumped permanently to the seawater tap of the laboratory. One tap provides approx. 10L/min. The inlet of 200L-barrel was connected with a T-split as short as possible to two taps and the flow was set to >2L/min. For the outlet of the barrel a larger diameter hosepipe was used to ensure an appropriate level of seawater in the barrel and was fixed at the sink.

The core "active" passive sampling device that is placed inside the 200L stainless steel barrel consists of a submersible pump which was mounted to a box with stainless steel square mesh (10mm eye size) with space for 4 silicon rubber sheets. Each with a dimension of 280x70mm. Two different kinds of silicone rubber passive samplers (SSP 125µm, Altesil 500µm) were used and two of each placed on one side for sampling on the stainless steel square mesh. Two temperature loggers were installed at the beginning and at the end of the silicon sheets to retrieve the actual temperature. First sampling started after flushing the barrel for 6h with seawater. The water sampling period was 4-5days.

A clean workspace was prepared with aluminium foil before changing the silicon rubber sheets. After sampling, the silicon rubber sheets were cleaned with seawater, dried with lint-free paper tissues and rolled with a tweezer in amber glass vials. All samples and field blanks were stored at -20°C.

5.2 Preliminary Results

5.2.1 Reflection Seismic - Examples

(C. Hübscher, H. Grob, H. Huster, J. Preine, E. Seidel)

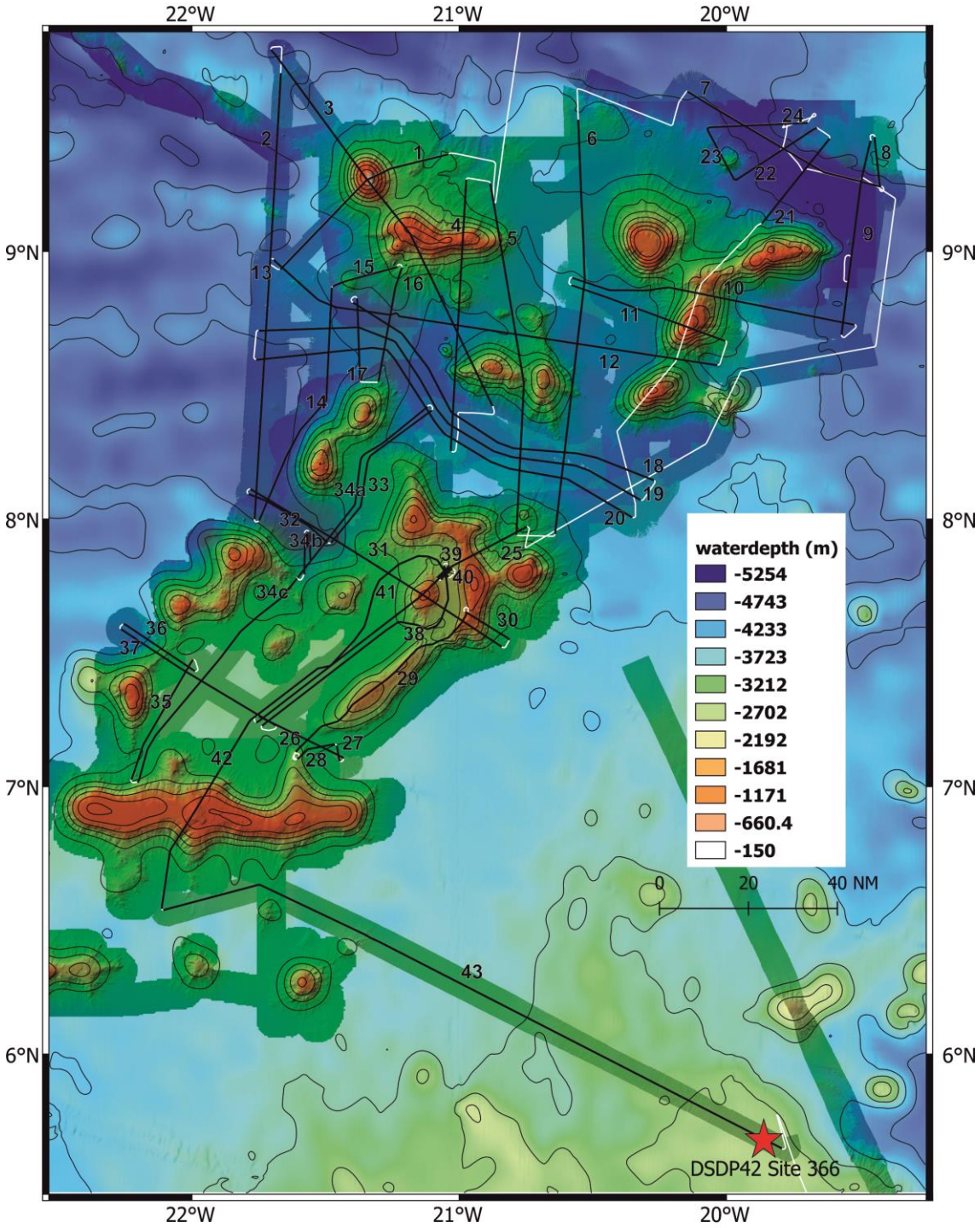

Fig. 5.2.1.1 Seismic base map with 50 m grid from RV MARIA S. MERIAN expedition MSM70 (van der Zwan et al., 2018) and RV METEOR expedition M152/2. Numbers correspond to profile number, for a complete list see chapter 7.2. White lines marks M152/2 ship track, superimposed by seismic profiles as black lines. Multibeam from M152/2 and MSM70 (van der Zwan et al., 2018) is plotted over ETOPO data.

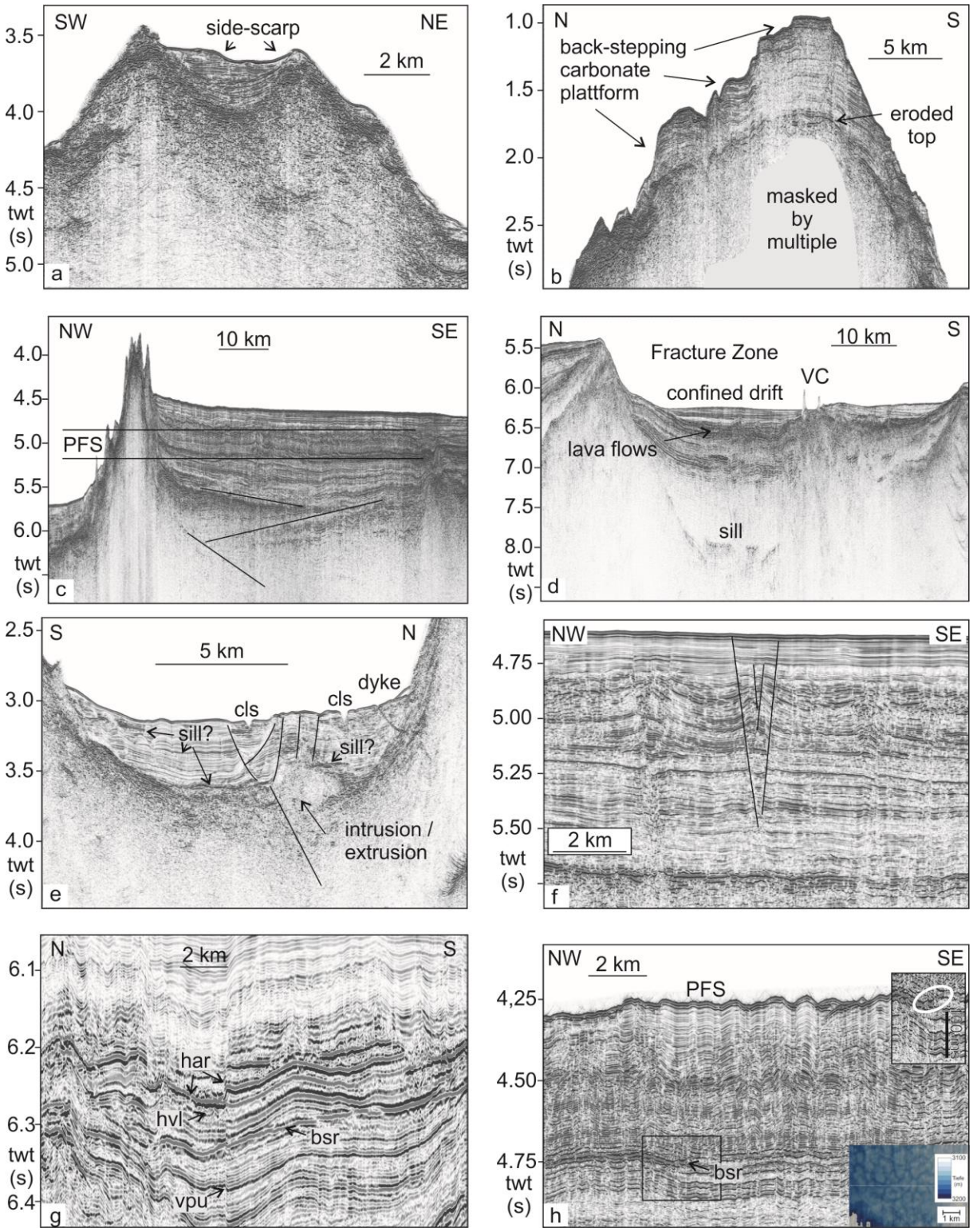

Fig. 5.2.1.2 Data examples. See text for discussion. Abbreviations; bsr: bottom simulating reflection, cls: channel levee system, har: high amplitude reflection, hvl: high velocity layer, PFS: polygonal fault system, VC: volcanic cone, vpu: velocity pull-up

We collected >4000 km of MCS data, distributed to 43 profiles (Fig. 5.2.1.1). Preliminary interpreted data examples are shown in Fig. 5.2.1.2a)-h). Just very few volcanos revealed a crater (Fig. 5.2.1.2a) or caldera. The summits of the higher volcanoes are eroded, partly covered by drowned, back-stepping and flat top carbonate platform (reefs) (Fig. 5.2.1.2b). Atoll forming was not observed. The present day depth of the tops will be taken to build a relative chronology. Onlap and downlap terminations of volcaniclastic sediments will be interpreted for the same purpose (Fig. 5.2.1.2c). The volcanic ridges evolved mainly on the shoulders of fracture zones, which control bottom current flow in some regions. These bottom currents in turn control drift deposition (Fig. 5.2.1.2d). Due to the high sediment thickness of up to 1 km faults are well resolved; most of them are listric or Y-shaped, suggesting strike-slip tectonics (Fig. 5.2.1.2e). Positive flower structure like fault systems are abundant (Fig. 5.2.1.2f). Many profiles show strong, BSR like reflections across the stratigraphy Fig. 5.2.1.2g). Depth beneath sea-floor and positive acoustic impedance contrasts rule out gas hydrate. Velocity pull-ups results presumably from high-velocity layers beneath a high-amplitude reflection horizon. According to the Initial Report from DSDP Leg 42 Site 366 which we crossed with profile 43 the BSR might represent a chert layer, which has been drilled 400 m beneath sea-floor. This corresponds well with a twt-intervall of 400-500 ms between BSR and sea-floor. The diagenetic front cross-cuts the stratigraphy, which explains the BSR characteristic. The chert seems to represent a stratigraphic boundary which prevents upward migration of fluids, as indicated by the low-frequency reflections in the south-eastern part of Fig. 5.2.1.2h).

5.2.2 Dredge Operations for Seafloor Sampling

(F.M. van der Zwan, M. Schade)

From a total of 14 deployed dredge casts, 9 returned with rock samples varying from Mn nodules in Kane Gap to volcanic rock samples, carbonates, phosphorites and Mn crusts from the Sierra Leone Rise. Volcanic rock samples were collected in 56% of the dredges that returned rock samples (Fig. 5.2.2.1).

Mn Nodules from Kane Gap were collected from areas with a high backscatter area on gentle slopes (Fig. 5.2.2.2). Two different types were collected. Samples from the higher areas adjacent to Kane Gap (6DR; Fig. 5.2.2.2b) consist of larger 5-12 cm in diameter Mn Nodules. Those are similar in size and appearance as nodules from MSM70-17DR found in Kane Gap in 2018. In contrast to that dredge, large composite-nodules were not found and only a few double nodules were collected. From the valley of Kane Gap (7DR; Fig. 5.2.2.2c) smaller 4-8 cm diameter nodules were collected. ¼ of these nodules consisted of double and multiple nodule groups. Many of the nodules were covered with cm-sized fragments, consisting of volcanic rock and mineral fragments, similar as found at the BSM during MSM70 (van der Zwan et al., 2018). Dredge 8DR, performed to ground truth for singular Mn nodules in the more sedimented area, visible in backscatter (low signal), parasound and seismic data, returned empty. Dredge 9DR on a slope with a high backscatter signal but more sediment than at 6DR and 7DR, visible in PARASOUND data also empty.

Bathymetry of the Sierra Leone Rise showed a highly sedimented environment with little rock exposure. Therefore samples from the Sierra Leone Rise could only be collected from two different types of environments, both on the southern side of the SLR: elevated areas on the main plateau and the flanks of this plateau.

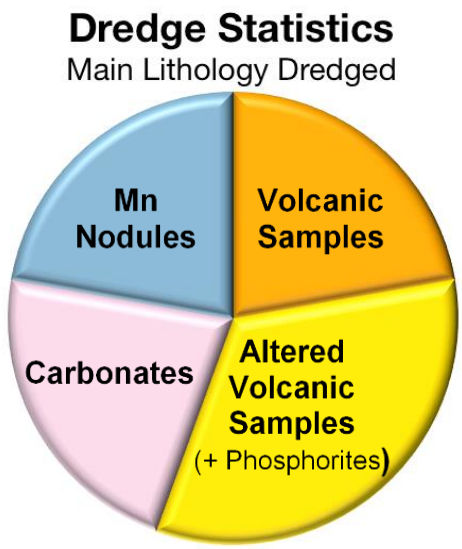

Figure 5.2.2.1 Main lithologies that were dredged during M152/2.

Dredges towed on circular elevations on the main plateau structure at depths <2000 m (14DR, 20DR; Fig. 5.2.2.3) returned carbonates from reef environments, consisting of rudstones and packstones with e.g. shell-, coral-, foram- and bacterial mat fragments and of fossil corals (Fig 5.2.2.4). Dredge 20DR from 2000-1700 m depth also collected younger organism (coral fragments, sponges, seastar, polipes). Evidence of chemically modified carbonates in the form of phosphorites was further found at the flanks of the SLR up to a depth of at least 3300 m.

These results showed that the complete Sierra Leone Rise is a guyot that has been close to sealevel after its formation. The greater depths of the carbonates compared to those found at the BSM (<2000 m), may imply an older age for the SLR.

At greater depths along the collapsed flanks of the Sierra Leone Rise volcanic samples could be retrieved. At depths between 2700 and 3600 m (14DR, 22DR, 24DR) highly altered, green, volcanic rock fragments and/or breccias were collected, in some cases consisting of altered glass (Fig. 5.2.2.5). Less strongly altered samples were collected from depths >3600 m (12DR, 28DR). These samples consist of a mixture of brecciated or fractured or unfractured vesicular (10-40%) basaltic volcanic samples, to massive non-vesicular aphyric to plagioclase phyric (up to 30% and max. 1.5 cm) basaltic-andesites. All samples are moderately to heavy altered and vesicles were regularly filled by alteration minerals.

Samples collected from all sites on the SLR were coated with up to 5 cm Mn crusts, indicating a higher age for all samples. A complete detailed description and photographs of all samples can be found in Appendix 12.1.

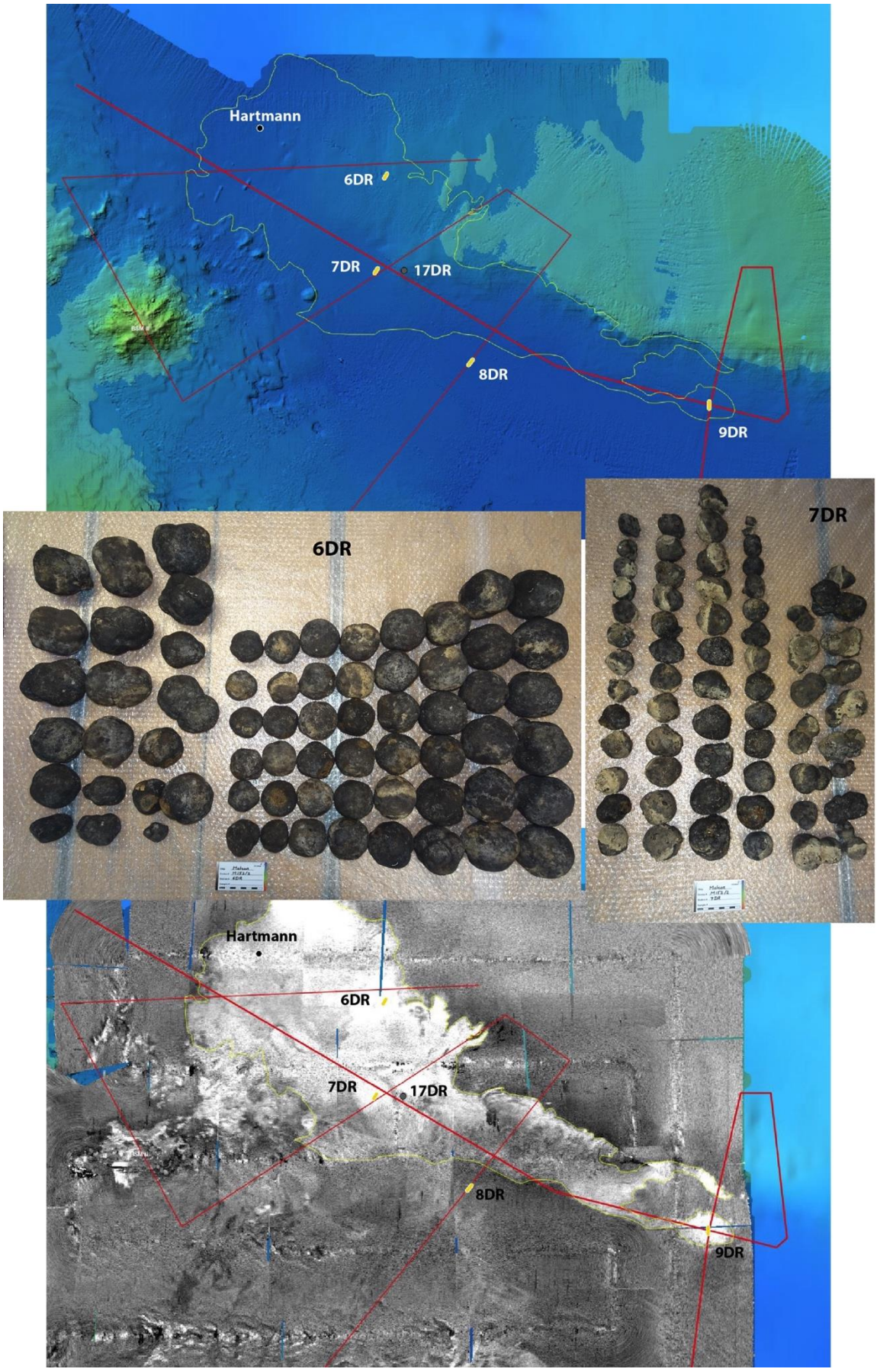

Fig: 5.2.2.2 Bathymetric map and backscatter results (high backscatter marked by light colours) of Kane Gap together with the locations of the dredges during M152/2, MSM70 and sampling position of Hartmann, 1989.

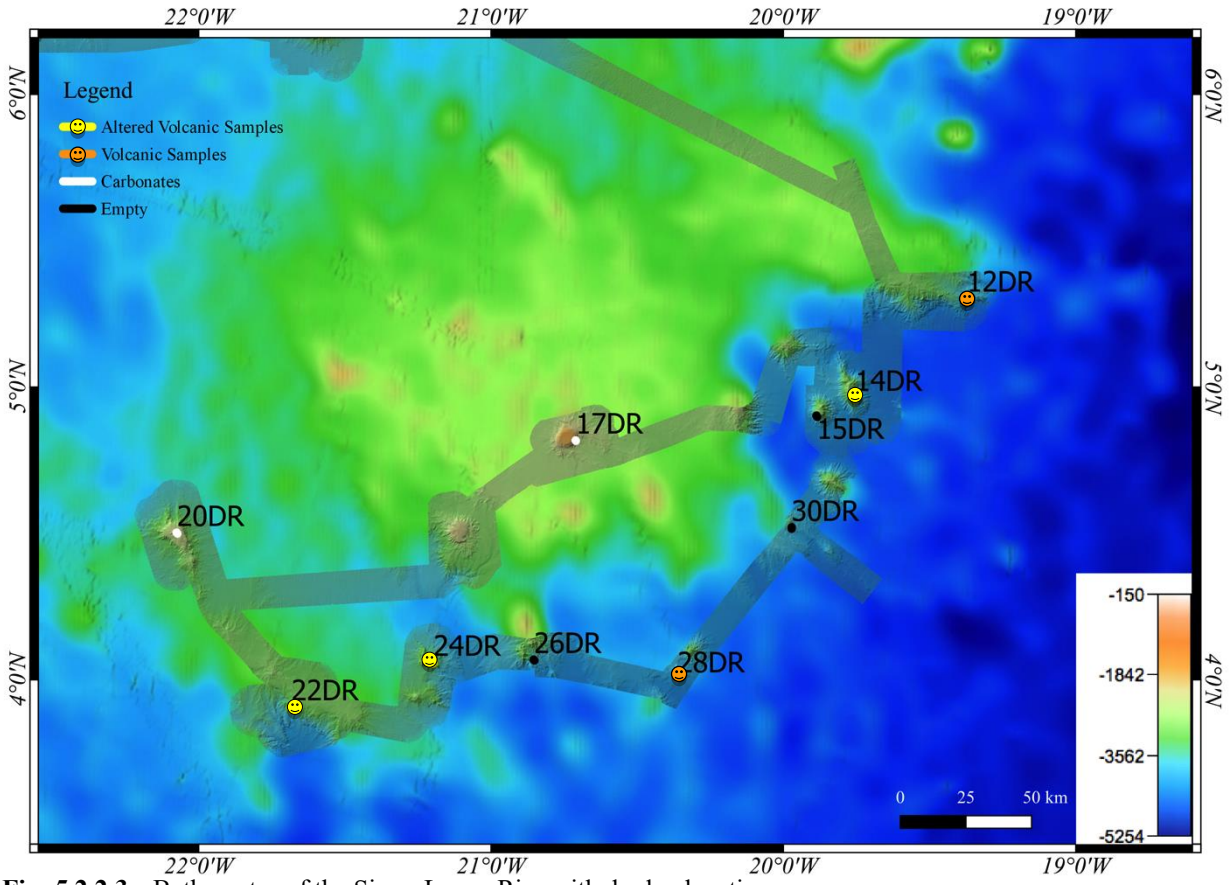

Fig: 5.2.2.3 Bathymetry of the Sierra Leone Rise with dredge locations.

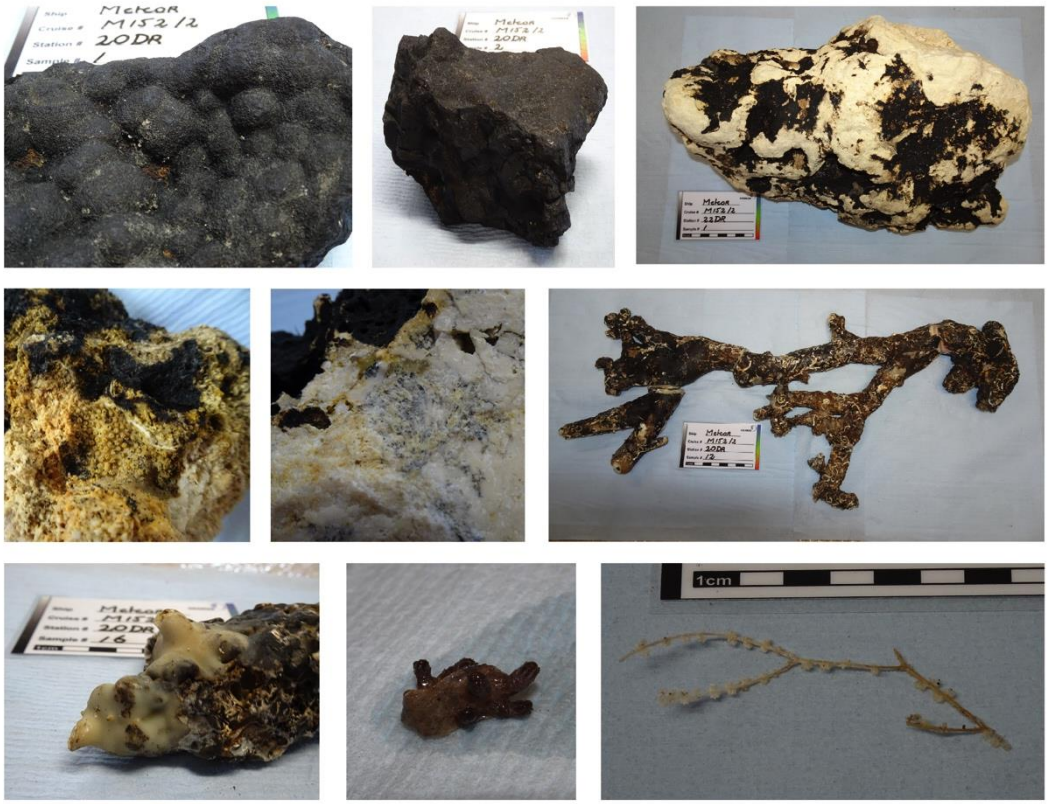

Fig; 5.2.2.4 Non volcanic rock samples: Manganese crusts (2x), phosphorite, close up of carbonate pack- and rudstones, old and younger corals, younger organisms.

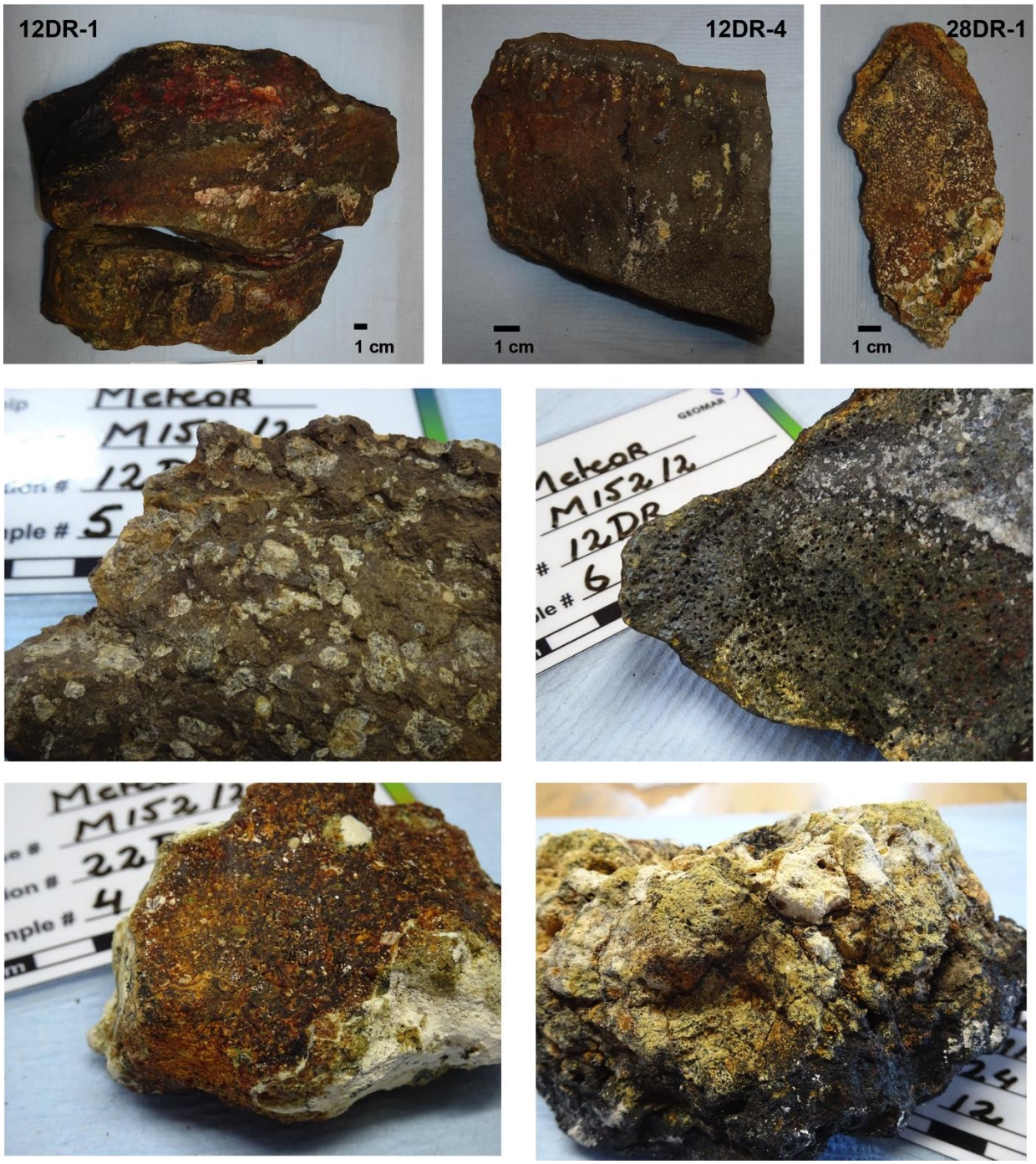

Fig: 5.2.2.5 Volcanic samples found at the Sierra Leone Rise: non-vesicular to vesicular aphyric basaltic andesites and basalts, close ups of a highly plagioclase phyric basaltic andesite and a vesicular basaltic andesite. Altered glass and completely altered phyric volcanic sample

5.2.3 Multibeam

(M. Schade, D. Lampridou)

Multibeam bathymetry data in the northern part of the working area was acquired during MCS-Profiles in between of the seamounts of the Bathymetrists Seamount Chain as well as by crossing selected seamounts e.g., Annan and Princesse Alice. During the mapping operation at the Sierra Leone Rise 3 carbonate platforms and 8 seamounts were mapped at the SLR (Fig. 5.2.3.1). In addition, some parts of the flanks of the SLR were mapped. The newly gained bathymetric record collected during expedition M152/2 covers a total area of 48,229 km^2, an area comparable to the area of the Dominican Republic.

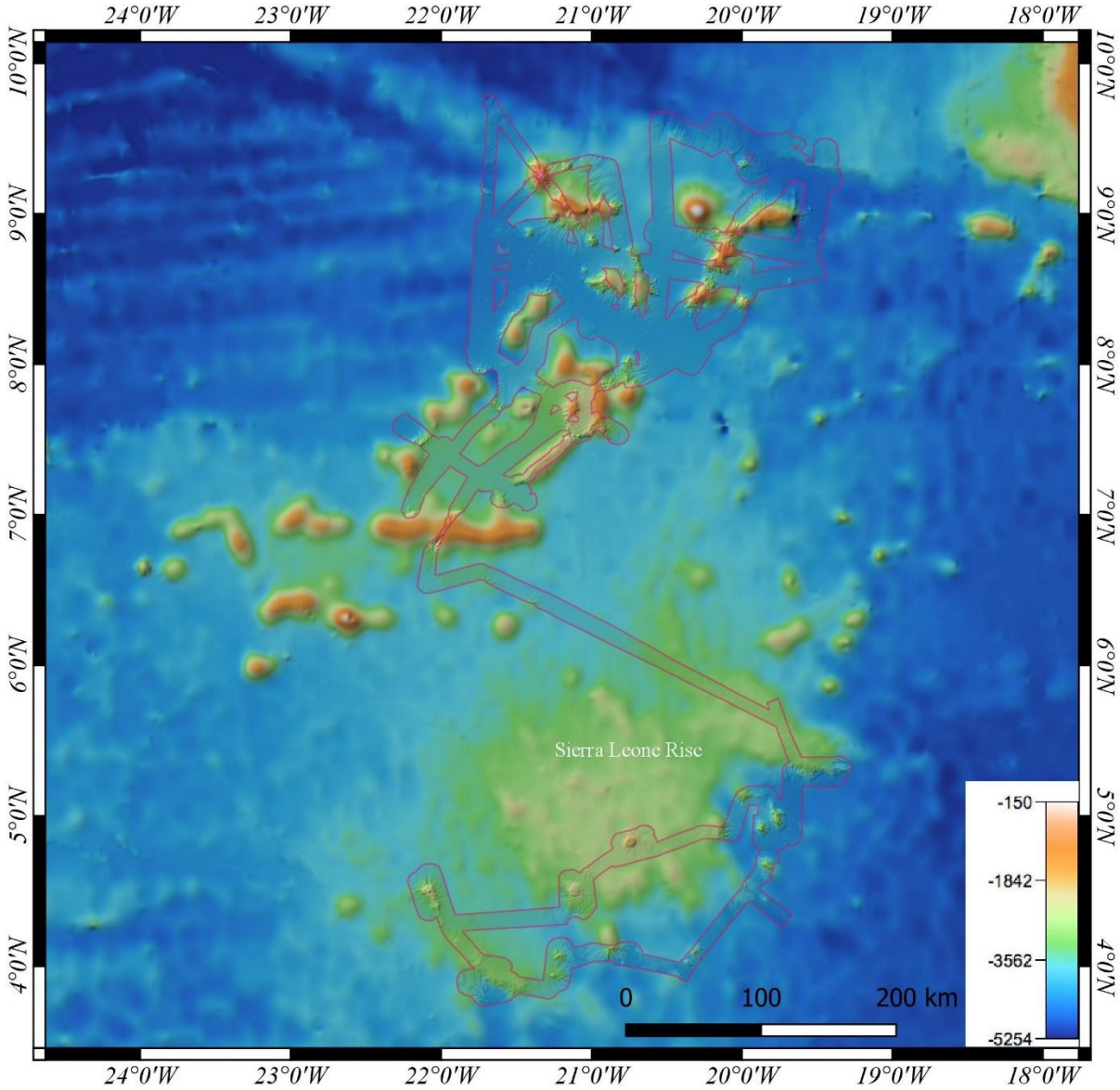

Fig. 5.2.3.1 Overview of the mapped area during Expedition M152/2. Difference between the background bathymetry compared to the newly gained data.

The ensonified area along the SLR revealed water depths ranging from 4.7Km up to 1.6Km. The northwestern area of the SLR shows complex seabed topography attributed to linear crosscutting features. The flanks of the identified nearly circular features show slope values more

than 30^0 (Fig. 5.2.3.2). The majority of them have pointy sharp summit area, while three of them are flat-topped due to carbonate platforms. Their diameter varies from 5 up to 8 km and their summit area deepens towards the west. Moreover, all of them depict erosional features along their flanks such as linear gullies and crescent-type scars, suggesting possibly slumping. and lack of sediment.

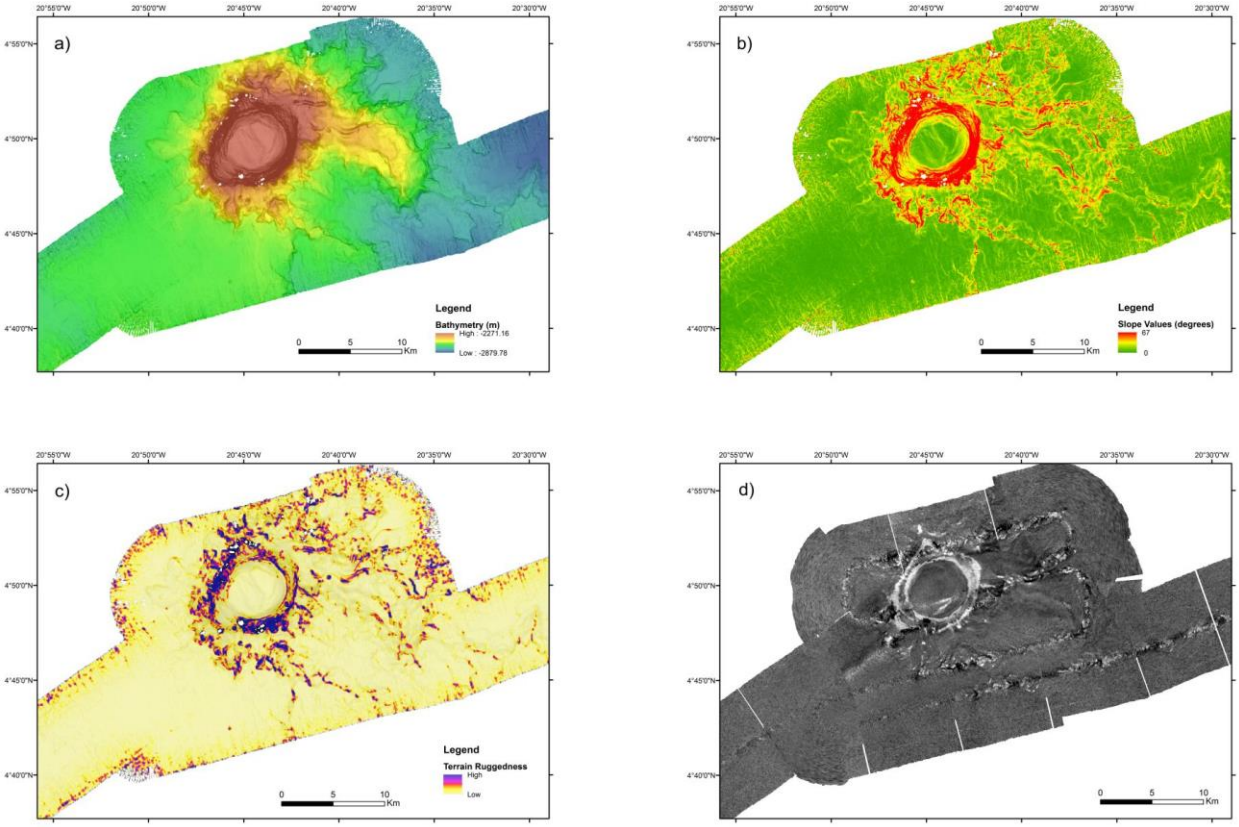

Fig. 5.2.3.2. a) Bathymetry map, b) Slope map, c)Terrain Ruggedness map, d) Backscatter map of flat-topped feature in the SLR

The top of the flat-topped features show significantly lower backscatter values to those found at the BSM, presumably owing to sediment drape. On the contrary, the incised channels along the flanks show a similar backscatter strength with the ones from the BSM area. It is noteworthy that the flanks of the circular features show really high backscatter values due to their steepness and lack of sediment.

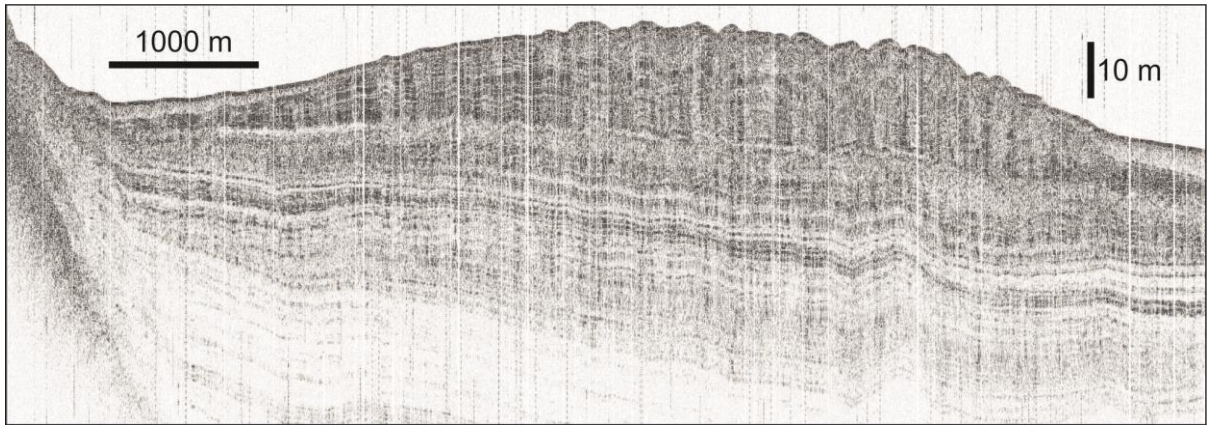

Fig. 5.2.4.1 PARASOUND data instance showing a contourite drift inside a fracture zone.

5.2.4 PARASOUND

(C. Hübscher)

Owing to the steep slopes data recovery and quality was generally rather poor in the BSM area. The data instance in Fig. 5.2.4.1 shows a contourite drift that emerged inside a fracture zone. The transparent and few meters thick layers at both sides are presumably mass transport deposits. The hummocks characteristics might result from OPAL transition.

5.2.5 Magnetic Measurements

(H. Huster, J. Preine, C. Hübscher)

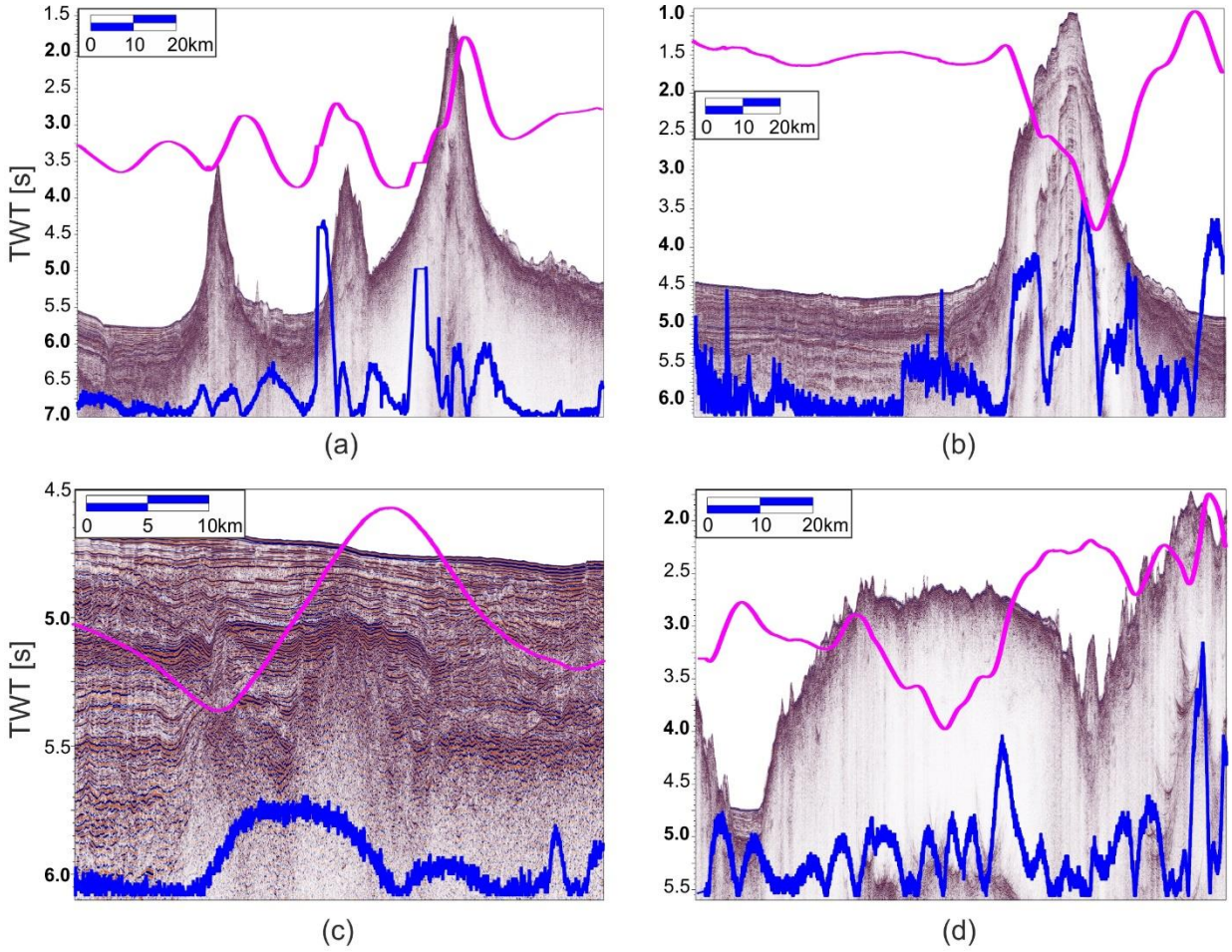

Fig. 5.2.5.1 Magnetic total field (light purple line) and gradient (blue line) plotted on top of seismic example profiles P04 (a), P42 (b), P26 (c) and P29 (d).

The magnetic will help to distinguish between magmatic and sedimentary structures and to estimate the depth of (cooled down) magma chambers. We plot here the total magnetic field (magenta) at the top and the gradient (difference between both sensors) below (blue). The total magnetic field reveals dipole style anomalies and the gradient highlights its lateral changes (Fig. 5.2.5.1 a-d). The seismic data in Fig. 5.2.5.1c show a high-amplitude reflection package, which is entirely covered by sediments. The magnetic anomaly proves its magmatic origin. The seismic line in Fig. 5.2.5.1d runs along the crest of a more than 60 km long, elongated volcanic ridge.

The total field indicates one major dipole anomaly or magma chamber, however, the gradient suggests 5-6 chambers or compartments.

5.2.6 Water and Air Sampling

(L. Kretzschmann)

In total 29 air samples and 3 field blanks were recovered. 61 polyurethane foam (PUF) plugs which usually turn their colour from white to slightly yellow during sampling and 32 quartz microfibre filters (QMA). All QMA north of the Sierra Leone Ridge were observed brown as shown in Figure 5.2.6.1. On several days, the chimney was blowing in the direction of the sampler for a short time. This was detected by a temperature sensor on a higher level above the bridge, so a possible contamination cannot be excluded and should be considered for data interpretation.

Fig: 5.2.6.1 ICA5 (north of the Sierra Leone Ridge, upper row) and ICA23 (south of the Sierra Leone Ridge, lower row)

For passive sampling of Persistent organic pollutants (POPs) in seawater 6 samples and 3 field blanks were recovered. For the first 3 samples and last 2 samples, the sampling was not stopped, because the ship was still moving with 3-6kn. Only ICW4 (Fig. 5.2.6.2) was interrupted very often, because of dredging. No problems occurred during the sampling periods.

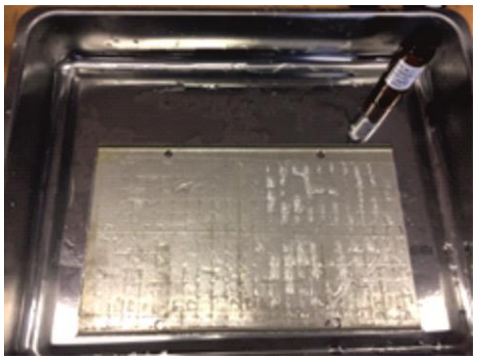

Fig: 5.2.6.2 Recovering of ICW1 (SSP, 125µm):

5.3 Outlook and Synopsis

(C. Hübscher, F. van der Zwan)

During RV METEOR expedition M152/2 we collected a rich geophysical data set without any malfunction. The multi-beam and high-resolution reflection seismic data are of excellent quality. After a first and very preliminary data analysis, we have to conclude that diagenesis, associated fluid flow and development of polygonal faults are abundant. The previously planned identification of faults, which developed as a consequence of plate tectonics will be handicapped because polygonal faulting overprinted tectonic faulting and vice versa. However, we do see that mapping and depth imaging of the identified diagenetic fronts bears the chance to develop a proxy for heat flow, which would help to unravel the magmatic and volcanic history of the BSM. The gravity data can potentially help us to test the hypothesis whether the lithosphere-asthenosphere boundary shallows from the SLR towards the BSM. The magnetic data will be used to estimate the distance between individual magma chambers beneath elongated seamounts. Both potential field data sets should be combined with wide angle reflection-refraction profiles in a future experiment.

A petrological and geochemical (major and trace elements, isotopes, Ar-Ar dating) study of the rock samples from the Sierra Leone Rise in comparison to the data already obtained for BSM samples of MSM70 (Long et al., in prep.), will give the opportunity to obtain an understanding of the igneous relation of the BSM and the SLR and their respective (or common) origins. Manganese nodules of Kane Gap will be geochemically studied (bulk analysis, Be-dating) together with samples of MSM70 (with S. Petersen), and related to their geological environment as observed by the seismic and bathymetric dataset to understand which geological and physiochemical conditions determine the growth and composition of manganese nodules.

6 Ships's Meteorological Station

(F. Otte, A. Raecke)

On the transit to Bathymetrists Seamounts about 830km west of Guinea / Sierra Leone, the FS Meteor initially sailed in a high pressure wedge that extended from a high centered over England to the Canary Islands. The wind was blowing from Northeast to East later backing North to Northeast with about 4 Bft and a significant wave height of 1.5 m. The research area was located at the northern end of the ITC zone, the latter extending from Sierra Leone up to the North coast of Brazil. By the time RV Meteor arrived, the research area was under the influence of the North/Northeast trade wind with 4 to 5 Bft and a significant wave height of 1.5 m from North. The ITC zone did not shift much in the following days and the RV Meteor remained at the edge of the Azores high until 10th of January with weakening winds of about 3 to 4 Bft. On the 11th of January the wind increased temporarily to 5 Bft, but on the following days it weakened again back to 3 to 4 Bft from the North. RV Meteor was still on the southern edge of a wide high pressure wedge part of an Atlantic high with good visibility experiencing a swell from North to Northwest with a significant wave height of 1.5 m. On the 18th of January the wind increased to 4 to 5 Bft, later that evening 6 to 7 Bft from northerly directions while the RV Meteor was on the way to a research area ca. 350 km further Northeast. This was caused by the move of the Acores high to the West which created higher pressure differences. The significant wave height also increased up to 2 m. On the next day up to midday the visibility was influenced by Saharan dust,

reducing to less than 8 km, later improving. In the morning of the 20th of January the wind decreased to 4 Bft. The significant wave height was now 1.5 m. Since research at this area had concluded, RV Meteor went back to the research area in the North. On the 21st of January, when RV Meteor arrived at the research area (at around 8°N 20,4°W), the weather was influenced by the Atlantic high pressure since the research area was still on the southern border of that high. That meant again wind from NNE with 4 Bft and a significant wave height from N to NE with 1.5 -2.0 m. The visibility was only a little reduced by the Saharan dust. Until the 25th of January the weather remained largely unchanged. On the 25th of January the research area was moved further to the South and closer to the ITC zone. In sunny weather with good visibility the wind decreased slowly and the significant wave height reduced to below 1.5 m. On the next day the wind continued to decrease to 3 to 2 Bft with a significant wave height below 1 m. Two swell components could be observed, one from the North and one from the South. On the 2&th of January RV Meteor arrived at about 5° N, coming closer to the ITC zone (from about 3°N to 5°S). The day started clear and cloudy with winds from North-Northwest 4 Bft increasing to 2 Bft later that evening. The wind sea almost calmed down completely. Only one swell component from Northwest continued with a height below 1m. On the night of the 30th of January the precipitation band of the ITC zone moved further North. For the first time on this voyage precipitation was observed with heavy showers and lightning. A total of 48 mm of rain was measured in just 4 hours. The wind was unchanged with 4 Bft from NNW and the significant wave height was 1 to 1.5 m. The wind speed and sea state remained unchanged over the next days. On the 1st of February research in this area was concluded and RV Meteor set course to Walvis Bay. The equator was crossed on the 2nd of February at 19.58 UTC. This day brought light winds from varying directions and a swell from SW less than 1 m. During the day there were heavy showers with cumulonimbus. In the early evening a tornado was observed in approximately 5 nautical miles distance from the ship which extended clearly to the surface of the water. The next day RV Meteor was still under influence of the tropical low pressure zone. After heavy showers in the morning the influence of the Southeast trade wind overtook. The wind changed to SSW with 4 Bft and the significant wave height was below 1.5 m from SSE. On the 4th of February RV Meteor left the area of influence of the low pressure zone. In front of South Africa arose a weak subtropical high. That meant the weather was influenced by a light Southeast trade wind, low convective clouds and a significant wave height of less than 1.5 m from South to Southeast. On the passage to Walvis Bay the high moved to the West. The wind continued to turn towards South with 2 Bft, in the first days there were still a few light showers: There was a swell component and a wind sea from southern directions less than 1.5 m. Air temperatures in the research area were constantly between 25° and 28°C and water temperatures were between 26° and 29°C. At the beginning of the voyage air temperatures were around 18°C in Las Palmas and on the passage to Walvis Bay temperatures reduced to 18°C, water temperature to 17°C. On the 11th of February RV Meteor arrived in Walvis Bay in the early afternoon with wind from the southwest.

7 Station List M152/2

7.1 Overall Station List

Station Number	Position (Start/End)	Date/ Time (UTC) Start/End	MSC-Profile #	Dredge #	Comment
M152/2_1-1 SEISTR	09° 20.9' /021° 03.8' 09° 28.7' /020° 32.4'	07.01.19; 19:33 11.01.19; 15:14	P01-P06	---	Multi-Channel-Seismic profiling
M152/2_2-1 MAG	09° 35.5' /020° 32.6' 09° 27.8' /020° 11.8'	11.01.19; 17:28 11.01.19; 20:19	---	---	
M152/2_3-1 SEISTR	09° 35.0' /020° 07.0' 07° 59.9' /020° 20.3'	11.01.19; 22:36 18.01.19; 08:36	P07-P20	---	Multi-Channel-Seismic profiling
M152/2_4-1 MAG	08° 02.8' /020° 19.6' 08° 52.1' /020° 04.9'	18.01.19; 09:49 18.01.19; 15:37	---	---	
M152/2_5-1 SEISTR	09° 05.2' /019° 52.3' 09° 28.4' /019° 41.1'	18.01.19; 18:22 19.01.19; 10:13	P21-P24	---	Multi-Channel-Seismic profiling
M152/2_6-1 DRG	09° 29.9' /019° 46.5' 09° 27.7' /019° 46.3'	19.01.19; 12:14 19.01.19; 15:18	---		
M152/2_7-1 DRG	09° 22.4' /019° 47.0' 09° 22.6' /019° 46.8'	19.01.19; 16:36 19.01.19; 19:26	---		
M152/2_8-1 DRG	09° 17.5' /019° 41.9' 09° 17.7' /019° 41.7'	19.01.19; 20:34 19.01.19; 23:37	---		
M152/2_9-1 DRG	09° 15.1' /019° 29.1' 09° 15.4' /019° 29.0'	20.01.19; 01:13 20.01.19; 04:32	---		
M152/2_10-1 SEISTR	07° 57.8' /020° 43.8' 07° 38.5' /019° 46.5'	20.01.19; 17:26 27.01.19; 09:26	P25-P43	---	Multi-Channel-Seismic profiling
M152/2_11-1 MB_PS	05° 45.5' /019° 47.5' 05° 18.1' /019° 22.3'	27.01.19; 12:44 27.01,19; 21:47	---	---	Multibeam- and Parasound-Profiling
M152/2_12-1 DRG	05° 18.0' /019° 22.3' 05° 18.2' /019° 22.3	27.01.19; 21:56 28.01.19; 01:27	---		
M152/2_13-1 MB_PS	05° 15.2' /019° 39.8' 04° 57.5' /019° 45.3'	28.01.19; 03:53 28.01.19; 11:55	---	---	Multibeam- and Parasound-Profiling
M152/2_14-1 DRG	04° 57.6' /019° 45.3' 04° 57.9' /019° 45.3'	28.01.19; 12:05 28.01.19; 14:58	---		
M152/2_15-1 DRG	04° 53.9' /019° 53.1' 04° 54.1' /019° 53.2'	28.01.19; 16:32 28.01.19; 19:13	---		
M152/2_16-1 MB_PS	05° 01.1' /019° 50.2' 04° 49.1' /020° 42.1'	28.01.19; 20:11 28.01.19; 20:51	---	---	Multibeam- and Parasound-Profiling
M152/2_17-1 DRG	04° 48.0' /020° 42.5' 04° 49.1' /020° 42.7'	29.01.19; 09:36 29.01.19; 12:49	---		
M152/2_18-1 MB_PS	04° 49.6' /020° 42.9' 04° 21.9' /021° 08.8'	29.01.19; 13:26 29.01.19; 20:42	---	---	Multibeam- and Parasound-Profiling
M152/2_19-1	04° 21.7' /021° 08.8'	29.01.19; 20:44	---	---	Multibeam- and

MB_PS	04° 33.1' /022° 09.6'	30.01.19; 07:07			Parasound-Profiling
M152/2_20-1 DRG	04° 30.0' /022° 04.4' 04° 30.2' /022° 04.5'	30.01.19; 08:02 30.01.19; 10:08	---		
M152/2_21-1 MB_PS	04° 31.0' /022° 02.7' 03° 53.8' /021° 40.9'	30.01.19; 10:57 30.01.19; 21:42	---	---	Multibeam- and Parasound-Profiling
M152/2_22-1 DRG	03° 54.0' /021° 40.9' 03° 54.3' /021° 41.0'	30.01.19; 21:50 31.01.19; 00:37	---		
M152/2_23-1 MB_PS	03° 54.3' /021° 54.3' 03° 54.5' /021° 12.3'	31.01.19; 00:53 31.01.19; 06:54	---	---	Multibeam- and Parasound-Profiling
M152/2_24-1 DRG	04° 03.3' /021° 11.9' 04° 03.6' /021° 12.0'	31.01.19; 08:06 31.01.19; 10:43	---		
M152/2_25-1 MB_PS	04° 04.0' /021° 11.4' 04° 04.0' /020° 51.1'	31.01.19; 11:14 31.01.19; 15:13	---	---	Multibeam- and Parasound-Profiling
M152/2_26-1 DRG	04° 03.9' /020° 51.1' 04° 04.1' /020° 51.3'	31.01.19; 15:24 31.01.19; 18:06	---		
M152/2_27-1 DRG	04° 00.4' /020° 21.7' 04° 00.7' /020° 21.7'	31.01.19; 21:42 01.02.19; 00:47	---		
M152/2_28-1 MB_PS	04° 00.8' /020° 21.5' 04° 38.8' /019° 50.6'	01.02.19; 01:10 01.02.19; 05:25	---	---	Multibeam- and Parasound-Profiling
M152/2_29-1 DRG	04° 30.9' /019° 58.3' 04° 31.3' /019° 58.3'	01.02.19; 07:10 01.02.19; 10:18	---		

7.2 Seismic Profile Station List

Station Number	MCS Profile	Start Date	Start Time	Start Latitude	Start Longitude	End Date	End Time	End Latitude	End Longitude	Length
			[UTC]	[°N]	[°W]		[UTC]	[°N]	[°W]	[km]
M152/2_1-1 SEISTR	01	07.01.19	19:33	09° 20.9'	021° 03.8'	08.01.19	04:11	08° 56.0'	021° 39.0'	88.64
	02	08.01.19	05:00	08° 57.4'	021° 41.6'	08.01.19	13:15	09° 38.9'	021° 39.2'	79.78
	03	08.01.19	16:06	09° 44.5'	021° 41.2'	09.01.19	10:28	08° 24.8'	020° 51.6'	173.73
	04	09.01.19	16:22	08° 15.3'	021° 01.0'	10.01.19	04:12	09° 14.4'	020° 57.6'	123.11
	05	10.01.19	05:37	09° 14.4'	020° 52.1'	10.01.19	20:28	07° 57.3'	020° 46.3'	162.21
	06	10.01.19	22:22	07° 56.5'	020° 37.4'	11.01.19	15:14	09° 28.7'	020° 32.4'	170.94
M152/2_3-1 SEISTR	07	11.01.19	22:36	09° 35.0'	020° 07.0'	12.01.19	07:52	09° 14.3'	019° 25.2'	95.01
	08	12.01.19	08:47	09° 15.0'	019° 24.8'	12.01.19	10:13	09° 22.6'	019° 25.6'	14.62
	09A	12.01.19	11:36	09°	019° 26.9'	12.01.19	18:01	08° 53.3'	019° 31.7'	57.99

				24.1'						
	09B	12.01.19	19:56	08° 57.6'	019° 31.1'	12.01.19	23:20	08° 40.9'	019° 33.3'	41.63
	10	13.01.19	00:25	08° 43.2'	019° 30.8'	13.01.19	12:43	08° 53.6'	020° 33.6'	122.33
	11	13.01.19	13:13	08° 52.0'	020° 33.8'	13.01.19	21:20	08° 34.1'	021° 01.3'	79.39
	12	13.01.19	21:19	08° 34.1'	021° 19.8'	14.01.19	16:48	08° 57.5'	021° 40.6'	194.15
	13	14.01.19	17:06	08° 57.3'	021° 41.7'	15.01.19	03:58	07° 59.7'	021° 45.0'	107.07
	14	15.01.19	04:20	07° 59.9'	021° 43.8'	15.01.19	14:29	08° 51.3'	021° 27.8'	104.52
	15	15.01.19	14:42	08° 52.1'	021° 27.1'	15.01.19	17:27	08° 56.1'	021° 13.2'	30.83
	16	15.01.19	17:53	08° 55.5'	021° 12.2'	15.01.19	22:46	08° 31.0'	021° 17.2'	56.17
	17	15.01.19	23:54	08° 31.1'	021° 21.4'	16.01.19	03:38	08° 48.1'	021° 22.8'	37.87
	18	16.01.19	03:38	08° 48.1'	021° 22.8'	16.01.19	18:41	08° 08.4'	020° 15.9'	162.82
	19	16.01.19	20:00	08° 03.9'	020° 18.5'	17.01.19	15:06	08° 41.9'	021° 43.7'	198.31
	20	17.01.19	16:24	08° 35.4'	021° 44.1'	18.01.19	08:36	07° 59.9'	020° 20.3'	181.41
M152/2_5-1 SEISTR	21	18.01.19	18:22	09° 05.2'	019° 52.3'	18.01.19	22:54	09° 24.4'	019° 36.4'	46.39
	22	18.01.19	22:54	09° 26.8'	019° 39.9'	19.01.19	03:34	09° 15.7'	019° 56.9'	37.42
	23	19.01.19	03:34	09° 15.7'	019° 56.9'	19.01.19	06:00	09° 26.8'	020° 03.4'	24.20
	24	19.01.19	06:00	09° 26.8'	020° 03.4'	19.01.19	10:13	09° 28.4'	019° 41.1'	41.69
M152/2_10-1 SEISTR	25	20.01.19	17:26	07° 57.8'	020° 43.8'	21.01.19	07:00	07° 14.2'	021° 44.2'	142.93
	26	21.01.19	07:33	07° 51.3'	021° 44.1'	21.01.19	11:14	07° 06.3'	021° 25.7'	43.14
	27	21.01.19	11:46	07° 06.0'	021° 26.2'	21.01.19	12:15	07° 08.6'	021° 26.6'	7.49
	28	21.01.19	12:28	07° 09.0'	021° 27.7'	21.01.19	14:04	07° 05.6'	021° 35.8'	17.0
	29	21.01.19	15:39	07° 06.9'	021° 36.0'	22.01.19	01:42	07° 38.5'	020° 57.3'	100.72

	30	22.01.19	01:42	07° 38.5'	020° 57.3'	22.01.19	03:40	07° 32.9'	020° 48.2'	25.77
	31	22.01.19	04:16	07° 30.9'	020° 49.5'	22.01.19	16:16	08° 06.1'	021° 45.6'	126.25
	32	22.01.19	16:42	08° 05.1'	021° 46.2'	22.01.19	20:27	07° 54.4'	021° 28.8'	40.76
	33	22.01.19	20:42	07° 54.6'	021° 27.6'	23.01.19	03:46	0.8° 23.9'	021° 05.5'	75.19
	34A	23.01.19	04:06	08° 25.0'	021° 06.0'	23.01.19	13:25	07° 45.9'	021° 34.8'	94.45
	34B	23.01.19	17:01	07° 56.5'	021° 32.8'	23.01.19	18:11	07° 50.4'	021° 32.6'	12.56
	34C	23.01.19	18:17	07° 49.7'	021° 32.9'	24.01.19	06:00	07° 01.3'	022° 11.0'	120.6
	35	24.01.19	06:37	07° 91.2'	022° 12.7'	24.01.19	11:15	07° 27.5'	021° 59.3'	63.26
	36	24.01.19	12:01	07° 25.7'	021° 58.8'	24.01.19	15:20	07° 35.8'	022° 14.0'	34.03
	37	24.01.19	15:45	07° 34.8'	022° 14.9'	24.01.19	22:29	07° 13.4'	021° 40.4'	84.11
	38	24.01.19	23:20	07° 13.4'	021° 43.2'	25.01.19	10:05	07° 48.6'	021° 02.4'	116.97
	39	25.01.19	10:33	07° 48.6'	021° 01.9'	25.01.19	10:56	07° 46.9'	021° 03.6'	20.51
	40	25.01.19	11:23	07° 46.6'	021° 02.8'	25.01.19	12:30	07° 46.8'	021° 01.8'	
	41	25.01.19	12:32	07° 46.8'	021° 01.8'	25.01.19	18:10	07° 32.3'	021° 22.8'	62.69
	42	25.01.19	18:10	07° 32.3'	021° 22.8'	26.01.19	06:39	06° 32.4'	022° 05.9'	142.04
	43	26.01.19	06:39	06° 32.4'	022° 05.9'	27.01.19	09:26	07° 38.5'	019° 46.5'	285.12
									∑	**4047.82**

8 Data and Sample Storage and Availability

The hydroacoustic (multibeam bathymetry) data of the working area will be placed in the GEOMAR data management system to ensure safe archiving (responsible Dr. Augustin). Following interpretation and publication of the data, it will be transferred to a World Data Centre archive linked to the GeoMapApp project via EMODNet. After a moratorium period until February 2021, it will be available from the data management team on request. The transit data (multibeam bathymetry) will be provided to the AtlantOS Project and made public available shortly after the cruise.

All dredged rock samples will be placed in the sample repository of GEOMAR, Kiel. Access to samples is protected initially by a moratorium period until February 2025 for cruise participants, proponents and collaborators. After post-cruise research and publication, applications for the use of the rock samples, can be made to the University of Kiel and the data management team at Geomar (responsible Dr. van der Zwan).

Table 8.1 Overview of data availability

Type	Database	Available	Free Access	Contact
Hydrography (raw multibeam)	BSH	February 2019	February 2025	Christian.huebscher@uni-hamburg.de
Multi-channel seismic (raw)	DKRZ Hamburg and future national data base	August 2019	February 2025	Christian.huebscher@uni-hamburg.de
Parasound (raw)	BSH	February 2019	February 2025	Christian.huebscher@uni-hamburg.de
Gravity and Magnetic (raw)	DKRZ data base at University of Hamburg	August 2019	February 2025	Christian.huebscher@uni-hamburg.de
raw data ADCP	PANGAEA	August 2019	February 2025	Christian.huebscher@uni-hamburg.de

The geophysical data are store at the DKRZ (University of Hamburg). It is planned to establish a national data center for marine seismic data, which ensures a long-term accessibility of these data. So far, there is no data enter, which can ensure that for the next decades. The length of the data moratorium is based on the following experience. A first data processing and analysis yield a set of working hypotheses, which are than elaborated in the course of BSc- and MSc-theses. MSc-theses are accomplished ca. one to one and a half years after the cruise. Based on these revised hypotheses we develop a DFG proposal. If everything goes well, the proposal is ready for submission two years after the cruise. It is important to note that these proposal are very competitive, which means that submitting a proposal just on hypotheses which initiated the cruise proposal are usually not successful. Hence, the proposal has to be crafted with utmost care. Evaluation of the proposal lasts at least 6 month, sometime 12 month. If a PhD-position has

been granted, it lasts at least 3 month to find a good candidate, who starts working 4-6 month after proposal approval. We are now 3 years after the termination of the cruise. The PhD project lasts at least 3 years, data are published 3-4 years after the beginning of the PhD project. In order to protect the work by the PhD student, we will not provide free access to the data before February 2025, which is six years after the cruise. After post-cruise research and publication, applications for the use of the data can be made to Christian Hübscher.

9 Acknowledgements

We are grateful to master Detlef Korte and his great crew for their continued contribution to a pleasant and professional atmosphere aboard R/V METEOR. The cruise was financed by German Research Foundation (DFG).

10 References

Ballmer M. D., van Hunen J., Ito G., Tackley P. J., Bianco T. A., 2007, Non-hotspot volcano chains originating from small-scale sublithospheric convection, Geophysical Research Letters, 34, DOI:10.1029/2007GL031636

Ballmer M. D, Ballmer M. D., van Hunen J., Ito G., Tackley P. J., Bianco T. A., 2009 (updated version), Non-hotspot volcano chains originating from small-scale sublithospheric co nvection, Geophysical Research Letters, 34, http://www.mantleplumes.org/SSC.html, accessed on 07 June 2018, at 22:55

Emelyanov E. M. Elnikov I. N., Trimonis E. S., Kharin G. S., 1990, Geology of the Sierra Leone Rise, Geologische Rundschau, 79 (3), 823-848

Emery K. O., Uchupi E., Phillips J., Bowin C., Mascle J., 1975, Continental margin of off western Africa: Angola to Sierra Leone, Am. Assoc. Petroleum Geologists Bull., 59, 2209-2265

Fodor R. V., Hekinian R., 1981, Petrology of basaltic rocks from the Ceará and the Sierra Leone aseismic rises in the equatorial Atlantic Ocean, Oceanologica Acta, 4 (2), 223-228

Jones E.J.W., Goddard D.A., Mitchell J.G., Banner F.T. 1991. Lamprophyric volcanism of Cenozoic age on the Sierra Leone Rise: Implications for regional tectonics and the stratigraphic time scale. Marine Geol., 99, 19-28.

Jones E. J. W., McMechan G. A., Zeng X., 2015, Seismic evidence for crustal underplating beneath a large igneous province: The Sierra Leone Rise, equatorial Atlantic, Marine Geology 365, 53-60, https://doi.org/10.1016/j.margeo.2015.03.008

Kharin G.S., 1988, Igneous Rocks of the Submarine Sierra Leone Rise, Equatorial Atlantic. Okeanologiya 28, 1, 82–88.

King, S.D., Ritsema, J., 2000. African hot spot volcanism: small-scale convection in the upper mantle beneath cratons. Science 290 (5494), 1137-1140.

Knesel, K.M., Souza, Z.S., Vasconcelos, P.M., Cohen, B.E., Silveira, F.V., 2011. Young volcanism in the Borborema Province, NE Brazil, shows no evidence for a trace of the Fernando de Noronha plume on the continent. Earth and Planetary Science Letters 302 (1), 38-50.

Kumar N., Embley R. W., 1997, Evolution and origin of Ceará Rise: An aseismic rise in the western equatorial Atlantic, Geological Society of America Bulletin 88 (5), 683-694

Melson W. G., Jarosewich E., Cifelli R., Thompson G., 1967, Alkali Olivin Basalt dredged near St. Paul's Rocks, Mid-Atlantic Ridge, Nature, 215, 381-382

Peyve A.A., Skolotnev S.G. 2009. Alkali volcanism of the Bathymetrists Seamounts chain (Central Atlantic): Description and comparison. Dokl. Earth Sci. 425, 243–248. doi:10.1134/S1028334X09020159

Reusch, A., Nyblade, A., Wiens, D., Shore, P., Ateba, B., Tabod, C., Nnange, J., 2010. Upper mantle structure beneath Cameroon from body wave tomography and the origin of the Cameroon Volcanic Line. Geochemistry, Geophysics, Geosystems 11 (10).

Richter, F. M., and B. Parsons 1975. On the interaction of two scales of convection in the mantle, J. Geophys. Res., 80, 2529-2541

Sandwell D.T., Mueller R.D., Smith W.H.F., Garcia E., Francis R. 2014. New global marine gravity model from CryoSat-2 and Jason-1 reveals buried tectonic structure. Science 346, 65–

67. doi:10.1126/science.1258213

Schade, M., 2018. Structural and Geomorphological Connection of the Bathymetrists Seamounts and the Sierra Leone Rise, Central Eastern Atlantic. BSc-thesis, Christian-Albrechts-University of Kiel.

Skolotnev S.G., Kolodyazhny S.Y., Tsukanov N.V., Chamov N.P., Sokolov S.Y. 2009. Neotectonic morphostructures in the junction zone of the Cape Verde Rise and Cape Verde Abyssal Plain, Central Atlantic. Geotectonics 43, 51–66. doi:10.1134/S001685210901004X

Skolotnev S.G., Petrova V.V., Peyve A.A. 2012. Origin of submarine volcanism at the eastern margin of the Central Atlantic: Investigation of the alkaline volcanic rocks of the Carter Seamount (Grimaldi Seamounts). Petrology, 20, 1, 59-85.

Skolotnev S.G., Peyve A.A., Bylinskaya M.E., Golovina L.A. 2017. New data on the composition and age of rocks from the Bathymetrists Seamounts (eastern margin of the Equatorial Atlantic). Dokl. Earth Sci. 472, 1, 20-25.

Stakemann, J., 2016. Seismic and hydroacoustic characterisation of oceanic intraplate volcanoes on the Azores Archipelago. BSc-thesis at Institute for Geophysics, University of Hamburg, 132 pages

van der Zwan F.M., Scientific Party of MSM70 & Garbe-Schönberg, C.-D., 2018. BATHYCHEM: The Effect of Intraplate Volcanism on the Geochemical Evolution of Oceanic Lithosphere: Detailed Mapping and Sampling of the Bathymetrists Seamounts and Adjacent Fracture Zones – Crusie No. MSM70 – December 26, 2017 – February 01, 2018. MARIA S. MERIAN Berichte, MSM70, 133.p

Weiß, B., Hübscher, C., Wolf, D., Lüdmann, T., 2015.Submarine explosive volcanism in the southeastern terceira Rift / São Miguel Region (Azores). Journal of Volcanology and Geothermal Research 303, 79-91

11 Abbreviations

AB	Able-bodied Sailor
ADCP	Acoustic Doppler Current Profiler
BSM	Bathymetrists Seamounts Chain
BSR	Bottom simulating reflection
CAU	Institute for Geology / Christian Albrecht University Kiel
CTD	Conductivity, Temperature, Depth
CVR	Cape Verde Ridge
DWD	Deutscher Wetterdienst, Geschäftsfeld Seeschifffahrt / Hamburg
GFZ	Guinea Fracture Zone
Har	High-amplitude reflectionMAR Mid-Atlantic Ridge
Hvl	High-velocity layer
MB	Multi Beam
MM	Marine Mammal
MPI/M	Max Planck Institute for Chemistry, Mainz
MCS	Multi-Channel Seismic
NKUA	Department of Geology and Geoenvironment, National and Kapodistrian University of Athens
NMO	Normal moveout

POP	Persistent organic pollutants
PFS	Polygonal fault system
PS	PARASOUND
PUF	polyurethane foam
QMA	Quartz microfibre filter
UHH	Institute for Geophysics / University of Hamburg
SIS	Seafloor Information System
SLR	Sierra Leone Rise
SSC	Small-scale sub-lithospheric convection
SVP	Sound Velocity Profile
TBL	Thermal boundary layer
VFZ	Vema Fracture Zone
Vpu	Velocity pull-up
WCI	Water Colum Imaging
XBT	Expendable Bathythermograph
XSV	Expendable Sound Velocity Probe

12 Appendix

12.1 Rock Sample description and sample photographs

(F. van der Zwan)

Sample	Rock Type	Description	Size (cm)	Shape	Encrustations (mm)	Degree of Alteration (%)	Vesicularity (%)	Matrix Colour	Primary Minerals	Secondary Minerals	Remarks
6DR-1	Mn nodule	Nodule consisting of 5-6 round parts, strongly intergrown. 2 spots that may show connection to next nodule	7x6x6	Round irregular	rough surface (2 mm grains), <<1 mm carbonate						
6DR-2	Mn nodule	Nodule, round, 2 parts together	7x6.5x6.5	Round	relatively smooth surface (<1 mm grains). Minor <<1 mm carbonate						
6DR-3	Mn nodule	Nodule, round irregular, 4-5 halfround parts together	7x7x7	Round irregular	relatively smooth surface (<1 mm grains). <<1 mm carbonate						
6DR-4	Mn nodule	Nodule, round	7.5x7.5x7.5	Round	half rough (2 mm grains), half smooth						
6DR-5	Mn nodule	Nodule, round irregular, 7-8 parts together. 2 contact parts to other nodules	8.5x8.5x8	Round irregular	relatively smooth (<1 mm grains). White lines/spots						
6DR-6	Mn nodule	Noddle, round, smooth	9x9x8.5	Round	smooth to relatively smooth surface (<1 mm grains)						
6DR-7	Mn nodule	Nodule, consisting of 2-4 parts together, 2 parts smaller. One connecting nodule break	10x10x10	Round irregular	rough surface (2-3 mm grains), half smooth surface (smaller part)						
6DR-8	Mn nodule	Nodule, round, consisting of 6-7 parts, rounded.	10x9.5x9.5	Round	relatively smooth (<1 mm grains). White lines/spots						
6DR-9	Mn nodule	Nodule, elongated, consisting of two, nodules, flattened over 2-3 contact places	7x5.5x5	Elongated, irregular	relatively smooth (<1 mm grains)						
6DR-10	Mn nodule	Nodule, elongated, irregular, consisting of 5 nodule parts.	8x6x6	Elongated, irregular	smooth to relatively smooth surface (<1 mm grains), minor carbonate <<1 mm						
6DR-11	Mn nodule	Nodule, round with small nodule(s) on top	10x9x9	Round, bit irregular	smooth to relatively smooth surface (<1 mm grains), minor carbonate <1 mm						

6DR-12	Mn nodule	Nodule consisting of 2 nodules, overlap for 1/4	12x9x8	Elongated, irregular	relatively smooth to rough surface (<1-2 mm grains). Minor <<1 mm carbonate						
Sample	**Rock Type**	**Description**	**Size (cm)**	**Shape**	**Encrustations (mm)**	**Degree of Alteration (%)**	**Vesicularity (%)**	**Matrix Colour**	**Primary Minerals**	**Secondary Minerals**	**Remarks**
6DR-13	Mn nodule	Nodule consisting of 2 nodules (14 and 9 cm) attached to each other. 2 more contact points	14x9x9	Elongated, irregular	rough surface (2-3 mm grains), minor carbonate (<<1 mm)						Shark teeth on large nodule 8 mm
6DR-14	Mn nodule	Nodule consisting of >9 nodule parts.	9x9x8	Round irregular	relatively smooth (<1 mm grains). White lines/spots						
6DR-15	Mn nodule	Nodule consisting of 2 nodule parts. Multiple contact sides	7x7x7	Irregular round	smooth to relatively smooth surface (<1 mm grains), minor carbonate <<1 mm						Shark teeth 1 cm
6DR-16	Mn nodule	Nodule consisting of 2 nodule parts	8x7x7	Round, bit irregular	smooth to relatively smooth surface (<1 mm grains), minor carbonate <<1 mm						Shark teeth 1 cm
6DR-17	Mn nodule	Nodule consisting of multiple nodule parts + contact places	10x9x9	Round irregular	relatively smooth to rough surface (<1-2 mm grains). Minor <<1 mm carbonate, some white lines						Plant (sampled separately together with 6DR-Extra 49,50)
6DR-Extra 1-10		as 6DR-1,2									
6DR-Extra 11-20		as 6DR-3,4									
6DR-Extra 21-30		as 6DR-5,6									
6DR-Extra 31-40		as 6DR-7,8									
6DR-Extra 41		as 6DR-9,10									
6DR-Extra 42,43		as 6DR-11									
6DR-Extra 44-46		as 6DR-12									
6DR-Extra 44-46		as 6DR-12									
6DR-Extra 47,48		as 6DR-14									
6DR-Extra 49,50		as 6DR-15,16,17									Shark teeth + Plant: sampled separately
7DR-1	Mn nodule	Nodule with multiple <1 cm fragments, consisting of limestone/phosphorite and volcanoclastics	5x4x4	round irregular	relatively smoot (<1 mm grains) + 1/2 coarse sediment crust						

Sample	Rock Type	Description	Size (cm)	Shape	Encrustations (mm)	Degree of Alteration (%)	Vesicularity (%)	Matrix Colour	Primary Minerals	Secondary Minerals	Remarks
7DR-2	Mn nodule	Nodule with 1/2 covered in sediment with <1 cm black fragments	5.5x5x5	round	relatively smoot (<1 mm grains) + 1/2, 1 mm sediment crust + coarse fragments						
7DR-3	Mn nodule	Nodule with 1/2 multiple <1 cm fragments, consisting of limestone/phosphorite and volcanoclastics, in sediment	6x5x5	Round	smooth to relatively smooth surface (<1 mm grains) 1/2: 1-8 mm sediment with coarse fragments						
7DR-4	Mn nodule	Nodule with 1/2 multiple <1 cm fragments, consisting of limestone/phosphorite and volcanoclastics, in sediment	6x5.5x5.5	Round, elongated	smooth to relatively smooth surface (<1 mm grains) 1/2: 1-10 mm sediment with coarse fragments						Amph in fragments ?
7DR-5	Mn nodule	Nodule with multiple <1 cm black fragments, consisting of limestone/phosphorite and volcanoclastics	7.5x6x5	Round irregular	smooth to irregular with 1/4 up to a cm black fragment crust						
7DR-6	Mn nodule	Nodule with 1/2 covered in sediment with <1 cm black fragments	7x6x6	Round irregular	relatively smooth (<1 mm grains) with black cm sedimentmangan coated fragments						Amph as fragment
7DR-7	Mn nodule	Nodule with multiple <1 cm fragments, consisting of limestone/phosphorite and volcanoclastics	6.5x6x6	Round irregular	relatively smooth (<1 mm grains) with black cm sediment mangan coated fragments						
7DR-8	Mn nodule	Nodule with 1/3 multiple <1 cm fragments, consisting of limestone/phosphorite and volcanoclastics, in sediment	7x6x6	Elongated	relatively smooth (<1 mm grains) with black cm sediment mangan coated fragments						
7DR-9	Mn nodule	Nodule with 1/2 multiple <1 cm fragments, consisting of limestone/phosphorite and volcanoclastics, in sediment	7.5x7x7	Irregular	relatively smoot (<1 mm grains) + 1/2, 1 mm sediment crust + coarse fragments						Shark teeth
7DR-10	Mn nodule	Nodule with 1/2 multiple <1 cm fragments, consisting of limestone/phosphorite and volcanoclastics, in sediment	8x7x7	round	relatively smoot (<1 mm grains) + 1/2, 1 mm sediment crust + coarse fragments						
7DR-11	Mn nodule	Nodule with multiple <1 cm black fragments, consisting of limestone/phosphorite and volcanoclastics	8x7x6.5	Elongated, irregular	smooth to relatively smooth surface (<1 mm grains) 1/2 with coarse fragments						
7DR-12	Mn nodule	Nodule with multiple <1 cm black fragments, consisting of limestone/phosphorite and volcanoclastics	8x7x7	Elongated, irregular	smooth to relatively smooth surface (<1 mm grains) 1/2 with coarse fragments						

Sample	Rock Type	Description	Size (cm)	Shape	Encrustations (mm)	Degree of Alteration (%)	Vesicularity (%)	Matrix Colour	Primary Minerals	Secondary Minerals	Remarks
7DR-13	Mn nodule	Smooth Nodule	4.5x4x4	Irregular round	smooth						
7DR-14	Mn nodule	Smooth Nodule	6x6x5.5	Round	smooth with minor sediment						
7DR-15	Mn nodule	Smooth Nodule	8x7x6.5	Irregular	smooth with black cm fragments						
7DR-16	Mn nodule	Smooth Nodule	7x7x6	Round	mostly smooth to rough surface (up to 2 mm)						
7DR-17	Mn nodule	Double nodule, 1/4 overlapping	8.5x6x6	Elongated	smooth						
7DR-18	Mn nodule	Double nodule, 1/5 overlapping with 1/2 sediment with up to cm fragments of volcanoclastics	10x7x6	Elongated, irregular	relatively smoot (<1 mm grains) + 1/2 coarse sediment crust						Mica in sediment
7DR-19	Mn nodule	Nodule with small nodule on top with sediment with coarse grained fragments up to 1 cm	9x6.5x6.5	Elongated, irregular	relatively smoot (<1 mm grains) + 1/2 coarse sediment crust						
7DR-20	Mn nodule	Double nodule, 1/5 overlapping with 1/2 sediment with up to cm fragments of volcanoclastics	10x5x5	Elongated	relatively smoot (<1 mm grains) + 1/2, 1 mm sediment crust + coarse fragments						
7DR-21	Mn nodule	Combined (2-3) nodule with manganese crust	11x7x6.5	Irregular	relatively smoot (<1 mm grains) + 1/2, 1 mm sediment crust + coarse fragments						
7DR-22	Mn nodule	Combined 4-5 noodle with coarse sediment on half	10x7x6	Irregular	relatively smoot (<1 mm grains) + 1/2, 1 mm sediment crust + coarse fragments						
7DR-Extra 1-9		as 7DR-1-4									
7DR-Extra 10-16		as 7DR-5-8									
7DR-Extra 17-23		as 7DR-9-12									
7DR Extra 24-30		as 7DR-13-16									
7DR-Extra 31,32		as 7DR-17									
7DR-Extra 33,34		as 7DR-18									
7DR-Extra 35,36		as 7DR-19									
7DR-Extra 37,38		as 7DR-20									
7DR-Extra 39		as 7DR-21									
Sample	**Rock Type**	**Description**	**Size (cm)**	**Shape**	**Encrustations (mm)**	**Degree of Alteration (%)**	**Vesicularity (%)**	**Matrix Colour**	**Primary Minerals**	**Secondary Minerals**	**Remarks**

12DR-1	Volcanic block (2 pieces)	Massive block, coated with black, red, oker and white crusts. Slightly vesicular aphyric basalic-andesite (?)	25x15x6 + 21x8x5 + surface fragments	Blocky	<1 mm black (Mn), 1-2 mm Red-white-oker-brown encrustations (clay or Qtz): fault planes (?)	100% outside to 20% (?) inside	3% (elongated, up to 1 cmx3 mm)	light grey	na	surface crusts	Surface fault slip surface? Some lineations?
12DR-2	Volcanic block	Massive block, coated with black, red, oker and white crusts. Slightly vesicular moderately plagioclase phyric basalic-andesite (?)	16x15x8	Blocky	<1 mm black (Mn), 1-2 mm Red-white-oker-brown encrustations (clay or Qtz): fault planes (?)	100% outside to 20% (?) inside	1% (round, <2 mm)	light grey	Plagioclase (10%, <2 mm)	surface crusts	Surface fault slip surface? Some lineations?
12DR-3	Volcanic block	Massive block, coated with black and oker crusts. Slightly vesicular slightly plagioclase phyric basalic-andesite (?)	8x5x4	blocky	<1 mm black (Mn), oker-brown encrustations (clay or Qtz)	80% outside to 40 % inside	1% (round, <2 mm)	light grey to reddish	Plagioclase (3%, <3 mm, partially replaced)	Reddish alteration, alteration mineral of pl	
12DR-4	Volcanic block, top flow	Massive block, coated with black and oker crusts. Moderately vesicular aphyric basalic-andesite (?). Chilled margin on top 1/2-1 cm.	11x8x5	blocky	<1 mm black (Mn), Red-oker-brown encrustations (clay or Qtz)	80% outside to 50% inside	5% (elongated, <12x3 mm, perpendicular to top)	light grey	Plagioclase (needle microcrysts in bottom, 20%, <1 mm)	white, yellow, green vesicular filling (oa. Zeolites, chlorite?)	Top flow with chilled margin
12DR-5	Volcanic fragment	Highly plagioclase phyric, nonvesicular basaltic andesite (?) oker, brown altered.	10.5x5.5 x3	blocky	<1 mm dark brown encrustations (alteration front?)	100% outside to 70% inside	nonvesicular	coffeebr own	Plagioclase (30% <1.5 cm, mostly replaced)	Plagioclase alteration minerals: Qtz, and white mineral	
12DR-6	Volcanic fragment	Highly vesicular, aphyric basalt. Black, oker, red, white altered	10x8x7	blocky	<1 mm black (Mn), 1-2 mm Red-white-oker-brown encrustations (clay or Qtz)	100% outside to 60% inside	10-40% (round-irregular, <3 mm)	dark grey	Altered Ol (?) (1%, <2 mm)	Bubble filling, white, blue, red, yellow-green (glassy) (oa. Qtz, Zeolite, Chloride?)	Qtz surface at fracture
12DR-7	Volcanic fragment	Highly vesicular, aphyric basalt. Black, oker, red, white altered	9x6.5x5 x5	blocky	<1 mm black (Mn), Red-oker-brown encrustations (clay or Qtz)	100% outside to 50% inside	30% (roundish, <3 mm	dark grey	na	Zeolite vesicle filling, + Qtz + red, yellow, green alteration minerals (amorph)	Round surface structure with white needle minerals <1 mm
12DR-Extra 1-3		as 12DR-1,2									
12DR-Extra 4,5		as 12DR-4									
12DR-Extra 6,7		as 12DR-6,7									
12DR-Extra 8		Loose fragments <2 cm									
Sample	**Rock Type**	**Description**	**Size (cm)**	**Shape**	**Encrustations (mm)**	**Degree of Alteration (%)**	**Vesicularity (%)**	**Matrix Colour**	**Primary Minerals**	**Secondary Minerals**	**Remarks**

14DR-1	Manganese crust with breccia frangments attached	Manganese crust, irregular at top side, yellow-oker with black fragments on bottom (<2-3 mm): sediment/volcanic breccia?	8x7x3	crust	2 cm Mn crust	if volcanic then 100% altered	na	yellow	na	na	na
14DR-2	Manganese crust with breccia fragments attached	Manganese crust, rounded on top, bottom whitish-greenish fragments <2 mm thick. Carbonate/volcanics?	8x7x4	crust	4 cm Mn crust	na	na	white	na	na	na
14DR-3	Volcanic fragment	Middle grey volcanic fragment	3x2x1/2	fragment	1 mm rusty crust	0,3	1% (round, <1 mm)	middle grey	plagioclase (2%, <1 mm)	rusty minerals, white vesicle filling	na
17DR-1	Carbonate rudstone, covered with Mn crust	Carbonate rudstone with coral structures, dense, some smaller grains in between. Black dendritic structures, at the rims dark cofee brown. Coated with Mn crust	27x14x9	crust	Mn crust <1/2 cm, rusty in contact with carbonate		<1% (irregular)	white marble	carbonate		
17DR-2	Carbonate rudstone, covered with Mn crust	Carbonate rudstone with coral structures, dense, some smaller grains in between. Black dendritic structures, at the rims dark cofee brown. Coated with Mn crust	21x12x5	crust	Mn crust <1/2 cm, rusty in contact with carbonate		<1% (irregular)	white marble	carbonate		
17DR-3	Carbonate rudstone, covered with Mn crust	Carbonate rudstone with coral structures, dense, sediment pockets in the carbonate with carbonate sediment.. Black dendritic structures, at the rims dark cofee brown. Coated with Mn crust	24x9x6	crust	Mn crust <1 cm, rusty in contact with carbonate. Wavy surface.		<1% (irregular)	white marble	carbonate		
17DR-4	Carbonate rudstone, covered with Mn crust	Mn crust with carbonate, coral structure on the bottom, Mn coated	12x5x2	crust	Mn crust <1 cm, rusty in contact with carbonate		<1% (irregular)	white marble	carbonate		
17DR-coral		Younger reef plant/coral	80x0.4	long							
17DR-Extra 1-7		as 17DR-1-4									
17DR-Extra 8		Mn crust as 17DR1-4									
20DR-1	Mn crust	Mn crust with rusty bottom (carbonate contact), bobbly top (1-3 cm per round)	12x8x3	crust	smooth, bobbly surface						
20DR-2	Mn crust	Mn crust with rusty bottom (carbonate contact), flat top, multiple layers 3 mm to 1 cm thick	11x6.5x6	crust	smooth, flat (slightly wavy)						
20DR-3	Mn crust	Mn crust with rusty bottom (carbonate contact), bobbly top (1-2 cm per round)	7x6x2	crust	smooth, bobbly surface						
20DR-4	Carbonate packstone, Mn coated	Carbonate packstone with fragments of shells, corals, carbonate grains, mini polipen and younger sponses. Some larger coral fragments	21x17x12	irregular block	Mn coated < 1 mm		3%, round <1 mm	yellow white	carbonate		
20DR-5	Carbonate packstone, Mn coated	Carbonate packstone with fragments of corals, carbonate grains, mini polipen	18x10x9	irregular block	Mn coated < 1 mm		3%, round <1 mm	yellow white	carbonate		
Sample	**Rock Type**	**Description**	**Size (cm)**	**Shape**	**Encrustations (mm)**	**Degree of Alteration (%)**	**Vesicularity (%)**	**Matrix Colour**	**Primary Minerals**	**Secondary Minerals**	**Remarks**

20DR-6	Carbonate packstone, Mn coated	Carbonate packstone with fragments of corals, carbonate grains, bacterial mat, shells	7.5x6x4	irregular block	Mn coated < 1 mm		3%, round <1 mm	yellow white	carbonate		
20DR-7	Carbonate packstone, Mn coated	Carbonate packstone with fragments of corals, carbonate grains, mini polipen, shells	8x6x4	irregular block	Mn coated < 1 mm		3%, round <1 mm	yellow white	carbonate		
20DR-8	Carbonate pack-rudstone, Mn coated	Carbonate, half packstone (consisting of shell, coral, polipe, grains), half rudstone (consisting of large coral pieces; partially dissolved) Mn coated	17x13x8	irregular block	Mn coated < 1 mm; white cm x mm white elongated tubes		3-8% (round to irregular elongated <1 mm - 15x3 mm in pack to rudstone)	yellow white	carbonate		
20DR-9	Carbonate rudstone - Mn crust	Half carbonate rudsone (consisting of cm sized corals and radial features) and half Mn crust with 2-8 mm layers, partially rusty altered	24x18x8	irregular crust	Mn coated, < 1 mm to thick crust; some rusty spots.		1% (irregular, <3 mm)	white, black	carbonate, mn minerals		
20DR-10	Carbonate pack-rudstone, Mn coated	Carbonate, half packstone (consisting of coral, polipe, grains), half rudstone (consisting of large coral pieces; partially dissolved) Mn coated	11x10x6	irregular block	Mn coated < 1 mm; white cm x mm white elongated tubes		3-8% (round to irregular elongated <1 mm - 15x8 mm in pack to rudstone)	yellow white	carbonate		
20DR-11	Carbonate pack-rudstone, Mn coated	Carbonate, half packstone (consisting of coral, grains), half rudstone (consisting of coral pieces; partially dissolved) Mn coated	6.5x5x5	irregular block	Mn coated < 1 mm; white cm x mm white elongated tubes		3-5% (round to irregular elongated <1 mm - 15x8 mm in pack to rudstone)	yellow white	carbonate		
20DR-12	Fossile coral, Mn coated (6 pieces)	Coral, fossile, 10% dissolved, individual branches 2-5 cm. Coverd with elongated tubes and younger sponges. Inside white-pink	52x30x5	branched	Mn coated <2 mm; white cm x mm white elongated tubes		10% irregular, elongted 15x3 mm	white-pinkish	carbonate		
20DR-13	Fossile coral, Mn coated (2 pieces)	Coral, fossile, 15% dissolved, individual branches 3-6 cm. Coverd with elongated tubes and younger sponges. Inside white-grey	40x24x10	branched	Mn coated <1 mm; white cm x mm white elongated tubes		15% irregular, elongted 15x3 mm	white-grey	carbonate		
20DR-14	Fossile coral, Mn coated (3 pieces)	Coral, fossile, 3% dissolved, branch 1-2 cm. Mn coated coverd with elongated tubes. Inside white-pink	28x8x1.5	branched	Mn coated <2 mm; white cm x mm white elongated tubes		10% irregular, elongted 15x3 mm	white-pinkish	carbonate		
Sample	**Rock Type**	**Description**	**Size (cm)**	**Shape**	**Encrustations (mm)**	**Degree of Alteration (%)**	**Vesicularity (%)**	**Matrix Colour**	**Primary Minerals**	**Secondary Minerals**	**Remarks**

20DR-15	Fossile coral, Mn coated on carbonate packstone	Coral, fossile, 10% dissolved, individual branches 2-4 cm. Coverd with elongated tubes and younger life. Inside white-pink. Rudstone consisting of coral, polipen and grains.	24x20x9	branched	Mn coated <1 mm; white cm x mm white elongated tubes		10% round to irregular, elongted 15x3 mm	white-grey	carbonate		
20DR-16	Fossile coral, Mn coated with younger coral	Coral, fossile, 15% dissolved. Mn coverd with elongated tubes and younger white coral. Inside white-grey	9x5x4	branched	Mn coated <1 mm; white cm x mm white elongated tubes		15% irregular, elongted 15x3 mm	white-grey	carbonate		
20DR-17	Fossile coral, Mn coated	Coral, fossile, 30% dissolved. Mn coverd with elongated tubes. Inside white	8x2x2	branched	Mn coated <<1 mm; white cm x mm white elongated tubes		30% irregular, elongted 15x8 mm	white	carbonate		
20DR-18	Fossile coral, Mn coated	Coral, fossile. Mn coverd with elongated tubes. Inside white	7x2x1	branched	Mn coated <1 mm; white cm x mm white elongated tubes		na	white	carbonate		
20DR-Extra 1-3		as 20DR-1-3									
20DR-Extra 4-6		as 20DR-4-7									
20DR-Extra 7,9		as 20DR-8,10,11									
20DR-Extra 8		as 20DR-9									
20DR-Extra 10, 11		as 20DR-13									
20DR-Extra 12-17		as 20DR-17									
20DR-Extra 18		as 20DR-18									
20DR-Biology		Young organisms, conservated in ethanol, consisting of e.g. sponges, seastar, young coral, polipen)									
22DR-1	Phosphorite, Mn coated	Phosphorite crust with 1-3 cm wholes. Mn coated, some brown lines. Irregular layers 1-2 cm. Some dark mm grains	35x20x15	crust	Mn coated < 1 mm	100% phosphorite	<1% <1 mm round	white	phosphorite		
22DR-2	Phosphorite, Mn coated	Phosphorite crust with <1 cm holes, one completely through, widening to 2 cm Mn coated, some brown lines. Some dark mm grains	11x9x6	crust	Mn coated < 1 mm	100% phosphorite	<1% <1 mm round	white	phosphorite		
22DR-3	Mn crust with phosphorite	Mn crust, nops on top, also minor phosphorite. rusted against the phosphorite contact below, with little phosphorite 1/2 cm thick	9x8x6	crust	Mn crust 2-3 cm	100% phosphorite	Na	black, rust, white	Mn, phosphorite	Greasy brown minerals	
22DR-4	Altered (volcanic?) rock with Mn crust and phosphorite crusted	Altered sample consisting of altered greasy glassy rusty coloured minerals with darker and greenish minerals: altered glass? Mn coated, sides some phosphorite	6x5x2.5	rock fragment	Mn, < 1 mm on top, side up to 5 mm phosphorite	100% (glass?)	1%, <2 mm round	rusty		altered glass? Phosphorite, Mn	
Sample	**Rock Type**	**Description**	**Size (cm)**	**Shape**	**Encrustations (mm)**	**Degree of Alteration (%)**	**Vesicularity (%)**	**Matrix Colour**	**Primary Minerals**	**Secondary Minerals**	**Remarks**

22DR-5	Altered (volcanic?) rock with Mn crust and phosphorite crusted	Altered sample consisting of altered greasy glassy rusty coloured minerals with darker and greenish minerals: altered glass? + apple green rock, altered volcanic or phosphorite/Mn contact? Mn coated, sides some phosphorite	6x5x4	rock fragment	Mn, < 1 mm on top, side up to 5 mm phosphorite	100% (glass?)	1%, <2 mm round	rusty, green, white		altered glass? Phosphorite, Mn	
22DR-Extra 1		as 22DR-1									
22DR-Extra 2		as 22DR-2									
22DR-Extra 3		as 22DR-3									
24DR-1	Phosphorite, Mn coated	Phosphorite crust with <2 cm organic holes, some elongated, one completely through. Mn coated, some brown lines. Some dark mm grains	19x13x12	crust	Mn coated < 1 mm	100% phosphorite	<1% <1 mm round	white-pinkish	phosphorite		
24DR-2	Phosphorite, Mn coated	Phosphorite crust with <2 cm organic holes, some elongated, some completely through. Mn coated, some brown lines. Some dark mm grains	11x11x7	crust	Mn coated < 1 mm	100% phosphorite	<1% <1 mm round	white	phosphorite		
24DR-3	Phosphorite, Mn coated	Phosphorite crust with <2 cm organic holes, some elongated, some completely through. Mn coated (more than 1,2), some brown lines. Some dark mm grains	7x6x5	crust	Mn coated < 1 mm	100% phosphorite	<1% <1 mm round	white	phosphorite		
24DR-4	Phosphorite, Mn coated	Phosphorite crust with <1 cm organic holes, some elongated. Mn coated, some brown lines. Some dark mm grains	9x7x5	crust	Mn coated < 1 mm	100% phosphorite	<1% <1 mm round	white-pinkish	phosphorite		
24DR-5	Phosphorite, Mn coated	Phosphorite crust with <1 cm organic holes, some elongated, some completely through. Mn coated, some brown lines. Some dark mm grains	8x5x3	crust	Mn coated < 1 mm	100% phosphorite	<1% <1 mm round	white	phosphorite		
24DR-6	Phosphorite	Phosphorite crust with very shallow <1 cmelongated holes. Minor Mn coated, some brown lines. Some dark mm grains	6x5x3	crust	Mn coated < 1 mm	100% phosphorite	<1% <1 mm round	white	phosphorite		
24DR-7	Mn crust with altered volcanic fragments	Mn crust, 10 cm with nodular surface on breccia of vesicular altered volcanic fragments. Individual fragments up to 5 cm. Green and yellow altered.	46x22x15	irregular crust	Mn coated up to 10 cm	100% Mn and volcanics	10%, < 3 mm, round (volcanic samples)	apple green	not visible	apple green and oker volcanic alteration minerals, not individual visible	
24DR-8	Mn crust with minor altered volcanic fragments	Mn crust, 5 cm with organic surface on minor breccia of vesicular altered volcanic fragments. Individual fragments up to 3 cm, mm size thick. Green and yellow altered.	27x18x5	irregular crust	Mn coated up to 5 cm	100% Mn and volcanics	10%, < 3 mm, round (volcanic samples)	apple green	not visible	apple and dark green and oker volcanic alteration minerals, not individual visible	
Sample	**Rock Type**	**Description**	**Size (cm)**	**Shape**	**Encrustations (mm)**	**Degree of Alteration (%)**	**Vesicularity (%)**	**Matrix Colour**	**Primary Minerals**	**Secondary Minerals**	**Remarks**

24DR-9	Mn crust with minor phosphorite	Mn crust, with irregular surface and 30x2 mm fragments of phosphorite	13x8x7	irregular	Mn mostly	100% Mn and phosphorite	2%, <1 mm irregular	black and wite-yellow-black	phosphorite		
24DR-10	Mn crust with minor altered volcanic fragments	Mn crust, 5 cm with irregular surface on minor breccia of vesicular altered volcanic fragments. Individual fragments up to 2 cm, maybe continuous inside. Green and yellow altered.	13x11x5	irregular crust	Mn coated up to 5 cm	100% Mn and volcanics	10%, < 3 mm, round (volcanic samples)	apple green	not visible	apple green and oker volcanic alteration minerals, not individual visible	
24DR-11	Altered volcanic rocks, Mn coated	Completely apple green and oker altered vesicular rock. Breccia or fragmented, fragments up to 4 cm. Mn coated	15x11x5	irregular crust	Mn coated up to 2 cm	99% Mn and volcanics	10%, < 4 mm, round to irregular (volcanic samples)	apple green	not visible	apple green and oker volcanic alteration minerals, not individual visible. Maybe slightly less altered.	<1 cm patch of altered glass
24DR-12	Altered volcanic rocks, Mn coated	Completely apple green, creme and oker altered vesicular rock. Breccia or fragmented, fragments up to 2 cm. Mn coated	11x8x5	irregular crust	Mn coated up to 2 cm	100% Mn and volcanics	10%, < 3 mm, round (volcanic samples)	apple green, crème	not visible	apple green, cream and oker volcanic alteration minerals, not individual visible.	
24DR-13	Altered volcanic rocks, Mn coated	Completely apple green and oker altered vesicular rock. Breccia or fragmented, fragments up to 2 cm. Mn coated	13x8x5	irregular crust	Mn coated up to 1 cm	100% Mn and volcanics	10%, < 3 mm, round (volcanic samples)	apple green	not visible	apple green and oker volcanic alteration minerals, not individual visible	
24DR-14	Altered volcanic rocks, Mn coated	Completely apple green, creme and oker altered vesicular rock. Breccia or fragmented, fragments up to 2 cm. Mn coated	9x6x4	irregular crust	Mn coated up to 1 cm	100% Mn and volcanics	5%, < 2 mm, round (volcanic samples)	apple green	not visible	apple green, cream and oker volcanic alteration minerals, not individual visible.	
24DR-15	Altered volcanic rocks, Mn coated	Completely apple green and oker altered vesicular rock. Breccia or fragmented, fragments up to 2 cm. Mn coated	6x4x1.5	irregular crust	Mn coated <2 mm	100% Mn and volcanics	10%, < 4 mm, round (volcanic samples)	apple green	not visible	apple green, cream and oker volcanic alteration minerals, not individual visible.	
Sample	**Rock Type**	**Description**	**Size (cm)**	**Shape**	**Encrustations (mm)**	**Degree of Alteration (%)**	**Vesicularity (%)**	**Matrix Colour**	**Primary Minerals**	**Secondary Minerals**	**Remarks**

24DR-16	Mn crust with minor altered volcanic fragments	Mn crust, 6 cm with organic surface on minor breccia of vesicular altered volcanic fragments. Green and yellow altered. + recent biology	12x9x6	irregular crust	Mn coated up to 6 cm	100% Mn and volcanics	5%, < 2 mm, round (volcanic samples)	apple green	not visible	apple green and oker volcanic alteration minerals, not individual visible	1 cm x 1 mm organism growing on the rock
24DR-17	Phosphorite, Mn coated	Phosphorite crust with <1 cm organic holes, some elongated. Mn coated, some brown lines. Some dark mm grains. Organism on rock	7x6x4	irregular	Mn coated < 1 mm	100% phosphorite	<1% <1 mm round	white	phosphorite		1 cm x 1 mm organism growing on the rock
24DR-Extra 1-6		as 24DR-1-5									
24DR-Extra 7		as 24DR-7									
24DR-Extra 8		as 24DR-8									
24DR-Extra 9		as 24DR-9									
24DR-Extra 10-19		as 24DR-11-14									
24DR-Extra 20		fragments as 24DR-15									
28DR-1	Volcanic rock, altered, with little Mn coating	Brown partially altered vesicular volcanic rock, some parts apple green altered.Thin Mn coating	14x6x5	blocky	Mn coated < 1 mm	70% - 100% volcanics	30%, round, <2 mm	(red)brown	some black minerals <2 mm (?)	apple and dark green and oker volcanic alteration minerals, not individual visible	freshest rock of 24 and 28DR
28DR-2	Volcanic rock, altered, with little Mn coating	Partially altered vesicular volcanic rock, brecciated or fractures: fragments up to 3 cm, less altered. large parts apple green altered.Thin Mn coating.	21x12x8	blocky	Mn coated < 2 mm	80% - 100% volcanics	20%, round, <2 mm	(red)brown - apple green	some black minerals <2 mm (?)	apple and dark green and oker volcanic alteration minerals, not individual visible	
28DR-3	Volcanic rock, altered, with little Mn coating	Partially altered vesicular volcanic rock, brecciated or fractures: fragments up to 3 cm, less altered. large parts apple green altered. Mn crust.	25x8x7	irregular crust	Mn coated < 2 cm layered and nodular crust	90% - 100% volcanics	10%, round, <2 mm	(red)brown - apple green	some black minerals <2 mm (?)	apple and dark green and oker volcanic alteration minerals, not individual visible. Minor coffee carbonate/silica vein filling. White alteration minerals	
Sample	**Rock Type**	**Description**	**Size (cm)**	**Shape**	**Encrustations (mm)**	**Degree of Alteration (%)**	**Vesicularity (%)**	**Matrix Colour**	**Primary Minerals**	**Secondary Minerals**	**Remarks**

28DR-4	Volcanic rock, altered	Partially altered vesicular volcanic rock, brecciated or fractures: fragments up to 3 cm, less altered. large parts apple green altered.	8x6x5	irregular block	na	90% - 100% volcanics	10%, round, <2 mm (volcanics)	(red)brown - apple green	not visible	apple and dark green and oker volcanic alteration minerals, not individual visible.Striped. Minor coffee carbonate/silica vein filling.	
28DR-5	Volcanic rock, altered	Completely altered vesicular volcanic rock, brecciated or fractures: fragments up to 2 cm, less altered. large parts apple green and dark green veined altered. Abundant Si/Carbonate vein filling. Nodular Mn crust <1 cm	23x10x6	irregular crust	Mn coated < 1 cm	100% volcanics	10%, round, <2 mm (volcanics)	(red)brown - apple green	not visible	apple and dark green and oker volcanic alteration minerals, not individual visible.Striped. Abundant coffee carbonate/silica vein filling.	
28DR-6	Volcanic rock, altered	Completely altered volcanic rock, brecciated or fractures: minor fragments up to 2 cm, less altered. large parts apple green and dark green veined altered. Some Si/Carbonate vein filling. Nodular Mn crust <1 cm	13x8x5	irregular crust	Mn coated < 1 cm	100% volcanics	5%, round, <2 mm (volcanics)	(red)brown - apple green	not visible	apple and dark green and oker volcanic alteration minerals, not individual visible.Striped. Little coffee carbonate/silica vein filling.	
28DR-7	Mn crust with minor altered volcanic fragments	Mn crust, 2.5 cm layered with nodular surface on breccia of vesicular altered volcanic fragments, one less altered fragment. Individual fragments up to 3 cm. Green and oker altered.	14x13x4	irregular crust	Mn coated < 2.5 cm	90-100% Mn and volcanics	10%, round, <2 mm (volcanics)	(red)brown - apple green	not visible	apple and dark green and oker volcanic alteration minerals, not individual visible.	
28DR-8	Mn crust with minor altered volcanic fragments	Mn crust, 2 cm layered with nodular surface on altered volcanic fragments. Green and oker altered.	8x6x3	irregular crust	Mn coated < 2 cm	100% Mn and volcanics	na	apple green, oker	not visible	apple and dark green and oker volcanic alteration minerals, not individual visible.	
28DR-Extra 1		as 26DR-2									
28DR-Extra 2, 3		as 26DR-3,4									
28DR-Extra 4		as 26DR-5									
28DR-Extra 5,6		as 26DR-6									
28DR-Extra 7,8,9		as 26DR-7									

28DR-Extra 10, 11, 12	as 26DR-8									
28DR-Extra 13	fragments as 26DR-11-6									

12.2 Selected Pictures of Shipboard Operations

(J. Preine, H. Grob)

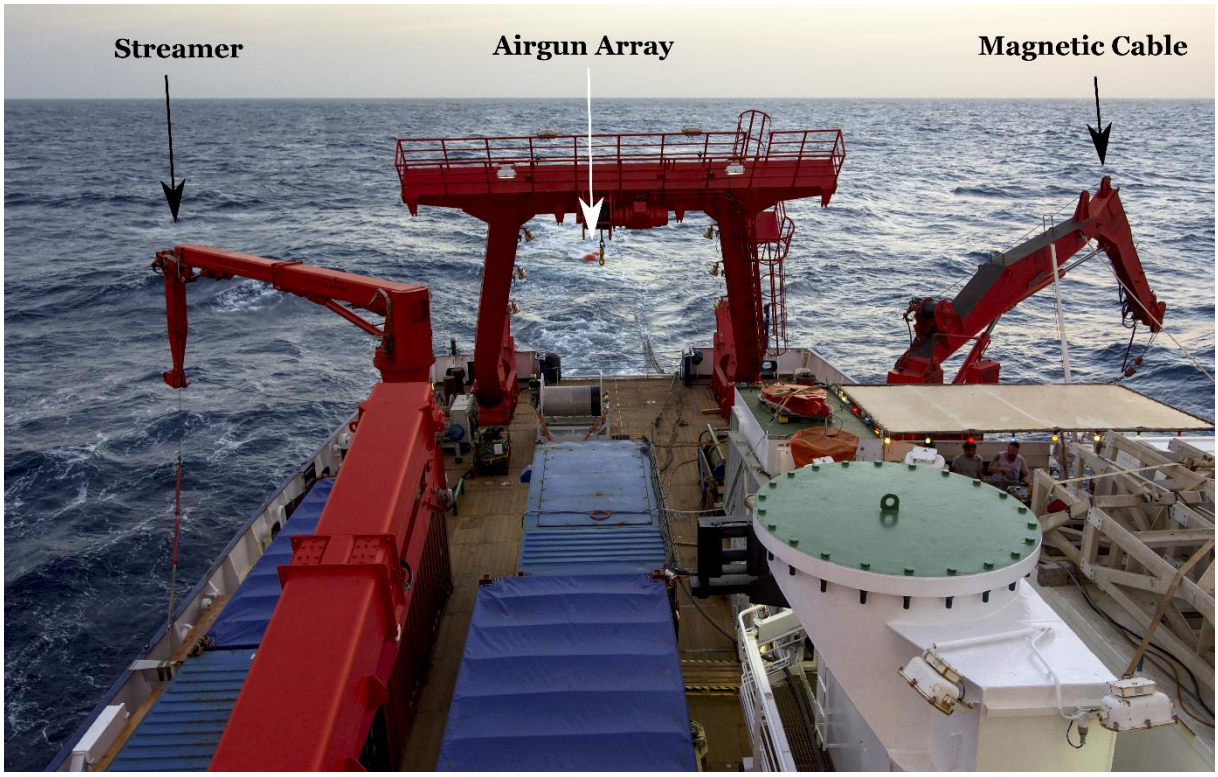

Fig. 12.2.1 Seismic and magnetics acquisition.

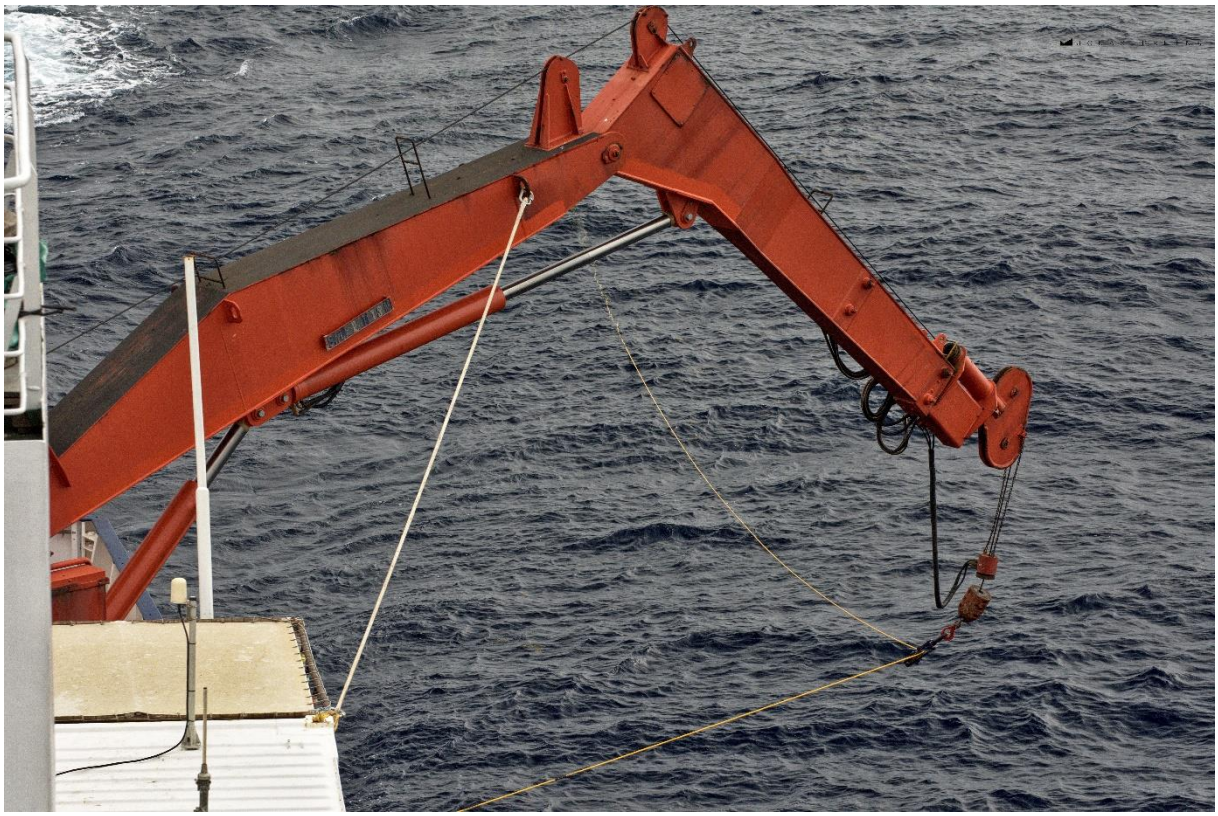

Fig. 12.2.2 Magnetic cable operated on portside.

Fig. 12.2.3 Magnetic winch operated on portside.

Fig. 12.2.4 Magnetic towfishes and connection cable ready for operation.

.